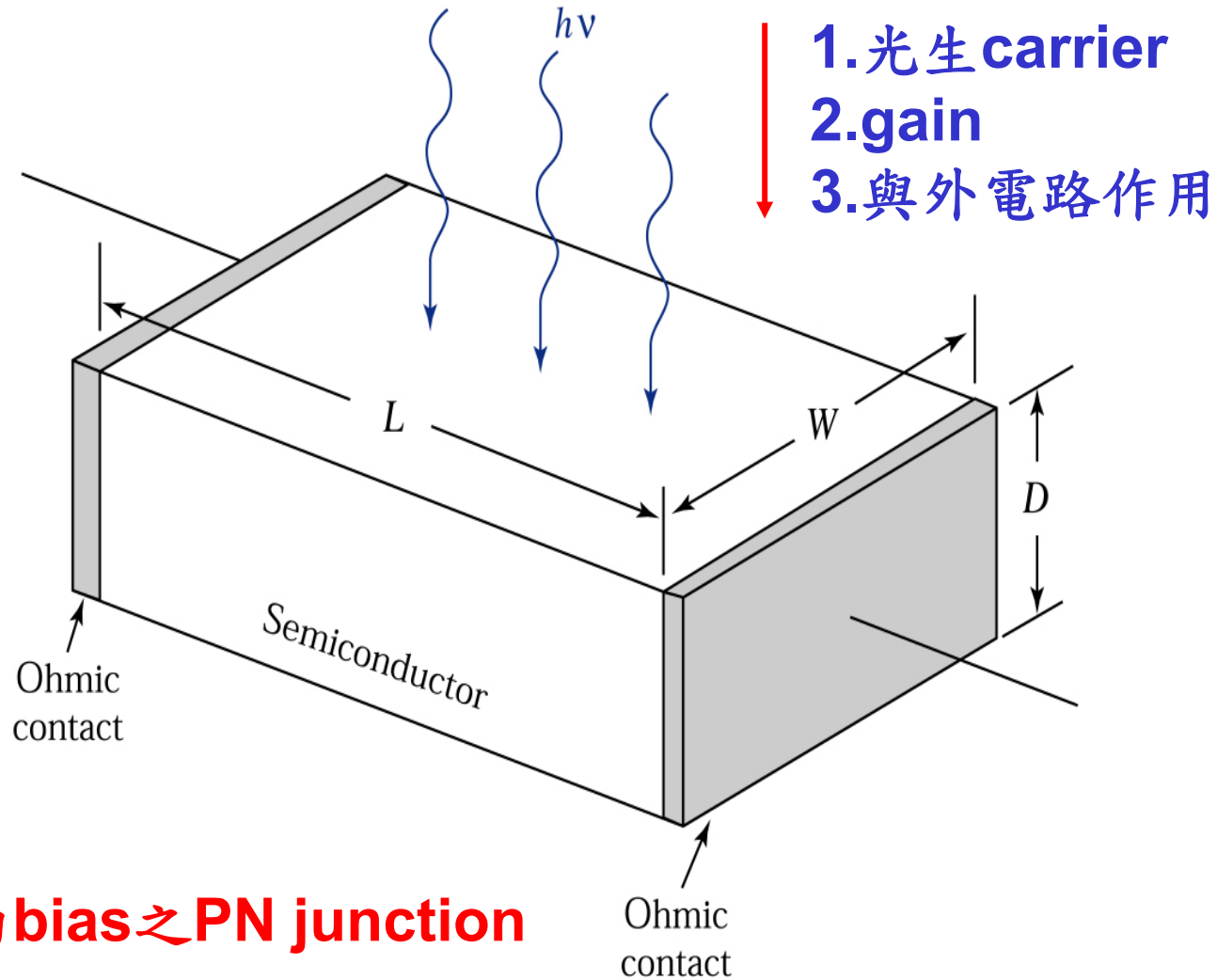

Semiconductor Devices

THIRD EDITION

S. M. Sze and M. K. Lee

Chapter 10

Photodetectors and Solar Cells



操作在反向bias之PN junction

Figure 10.1a. Schematic diagram of a photoconductor that consists of a slab of semiconductor and two contacts at the ends.

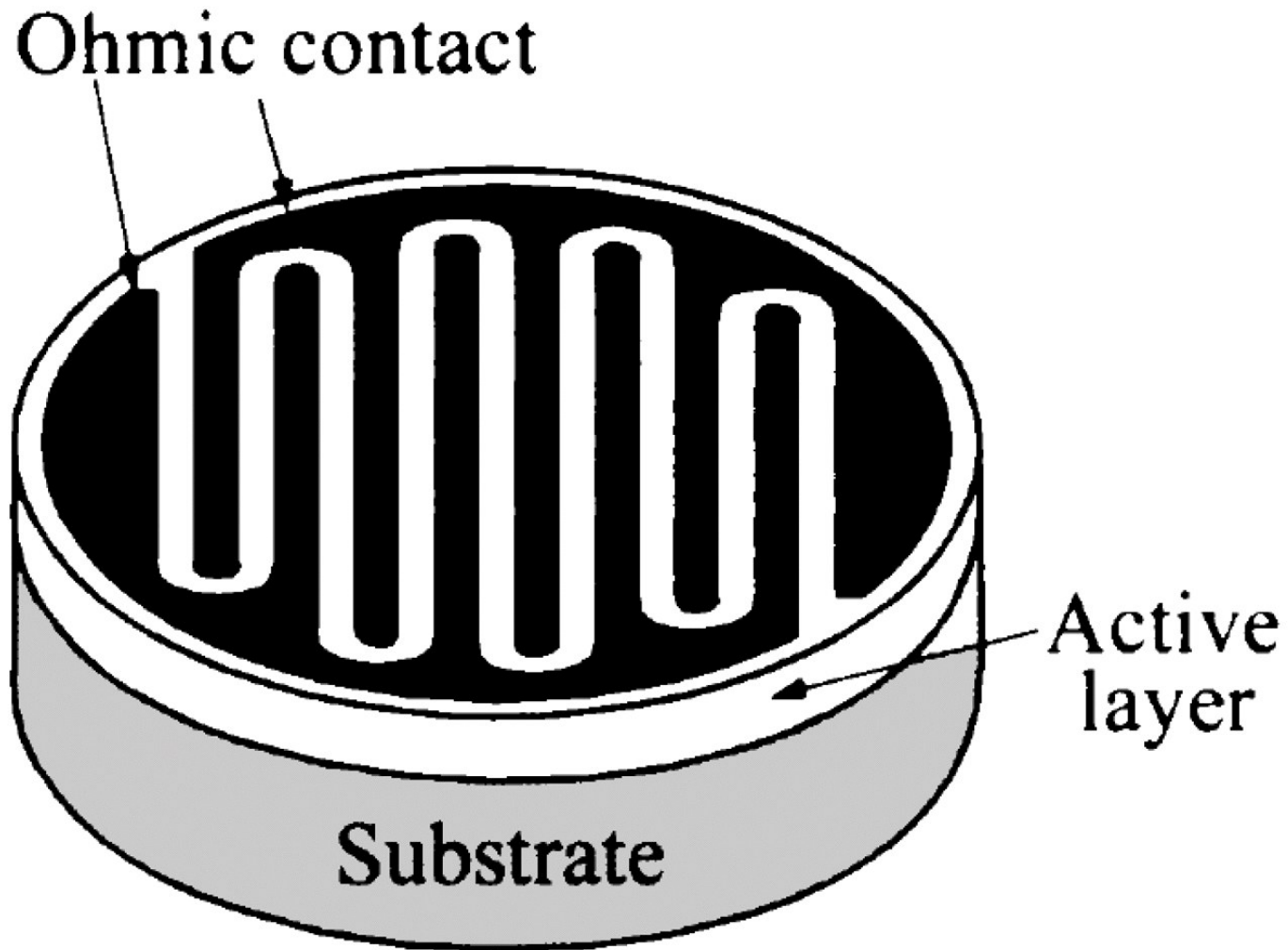
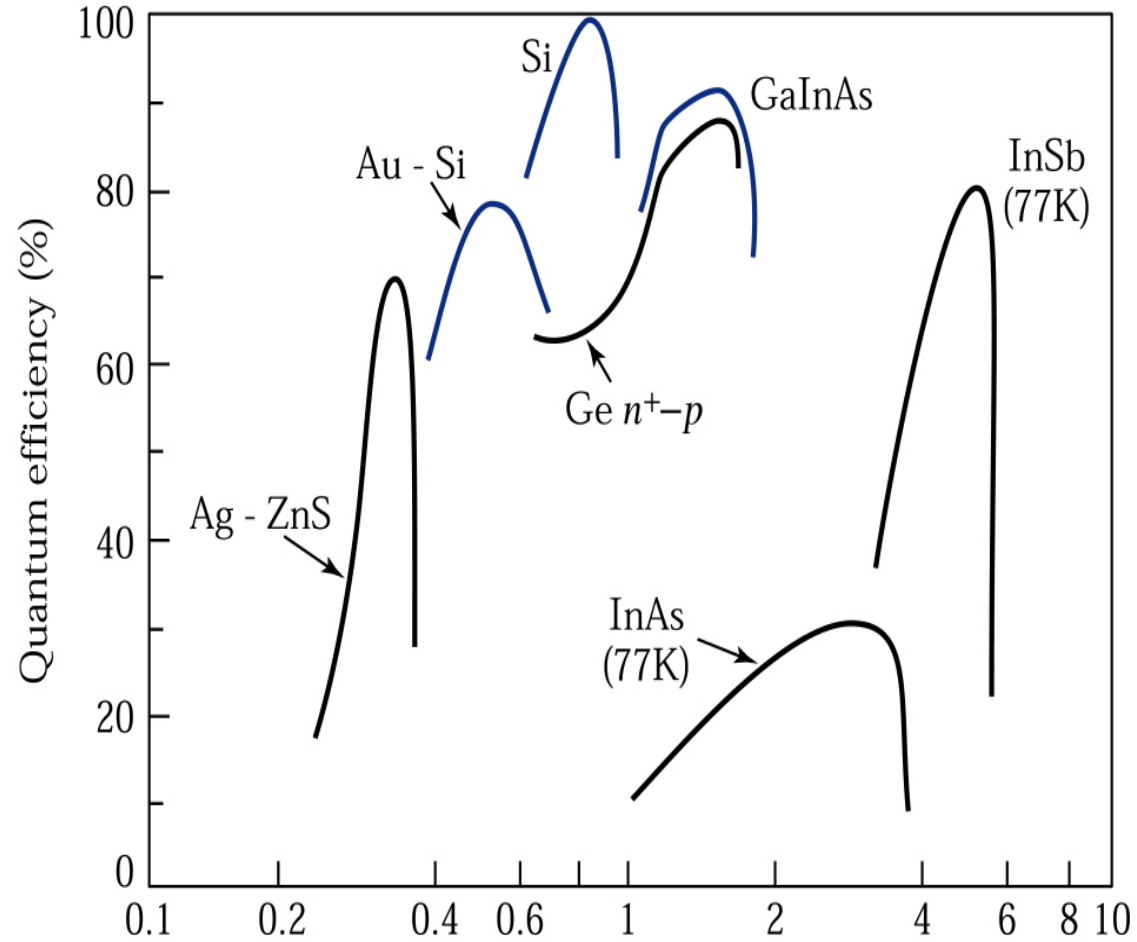


Figure 10.1b
© John Wiley & Sons, Inc. All rights reserved.

Layout: interdigit with a small gap



每個光子產生的e-h pair數 λ (μm)

Figure 10.2. Quantum efficiency versus wavelength for various photodetectors.^{21,22}

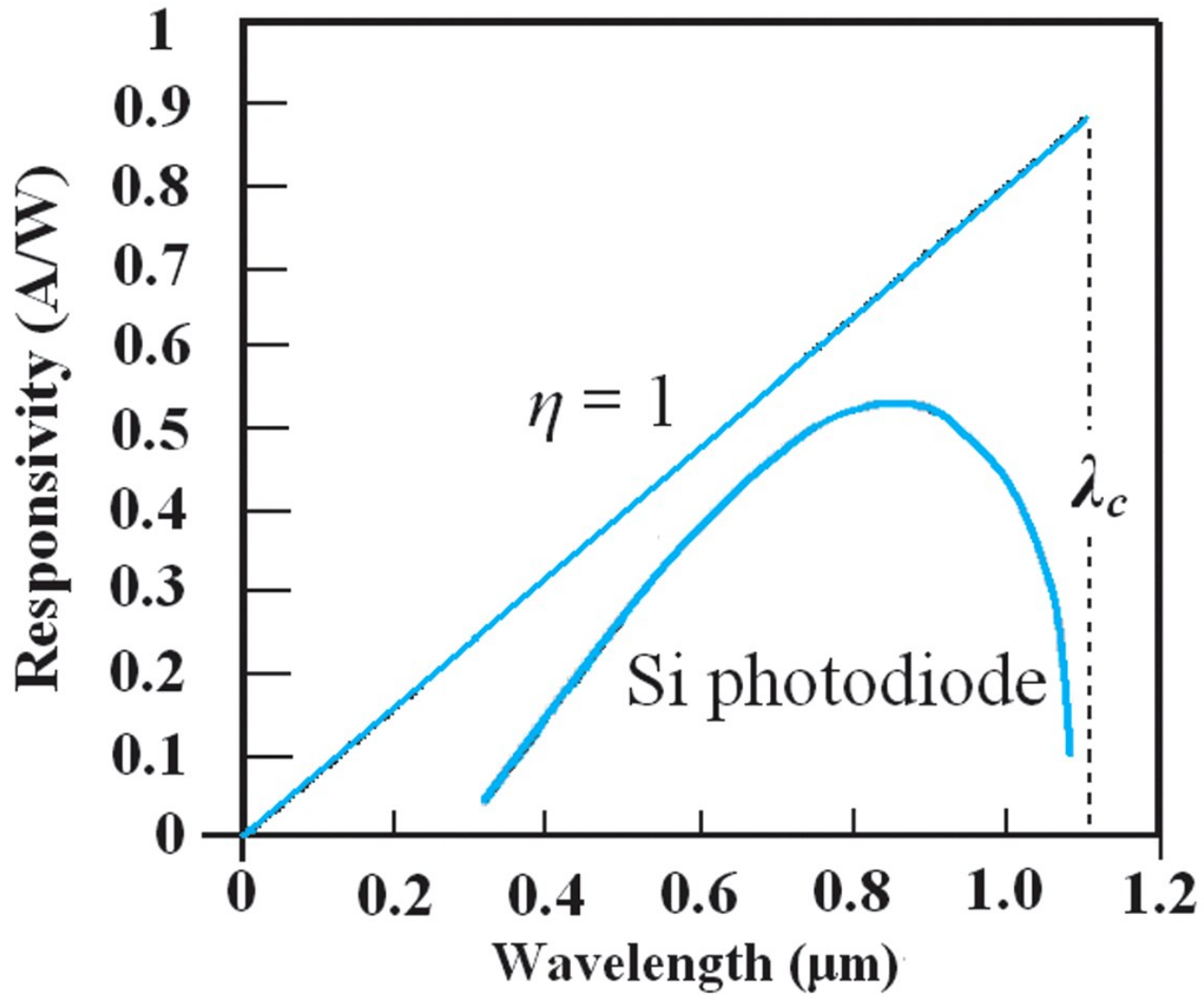


Figure 10.3
 © John Wiley & Sons, Inc. All rights reserved.

Ideal and typical commercial one

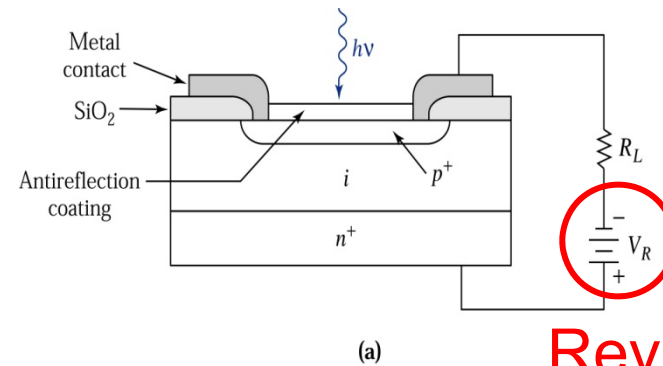
Figure 10.4.

Operation of a *p-i-n* photodiode.

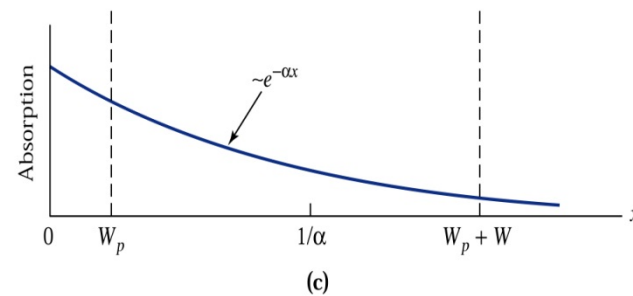
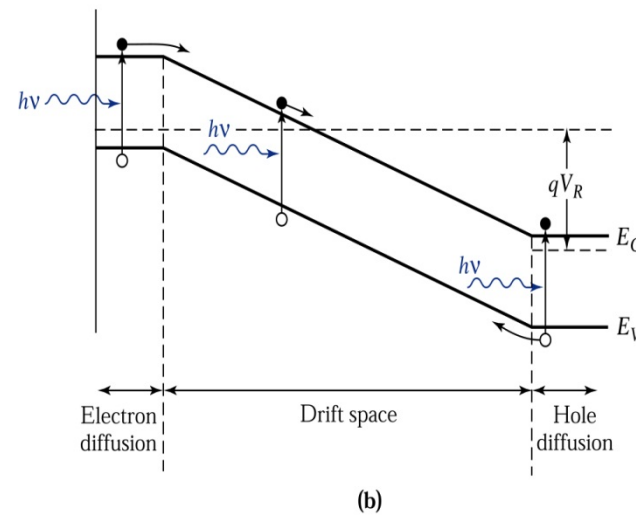
(a) Cross-section view of a **p-i-n** photodiode. (b) Energy band diagram under reverse bias.

(c) Carrier absorption characteristics.

最常用



Rev. bias



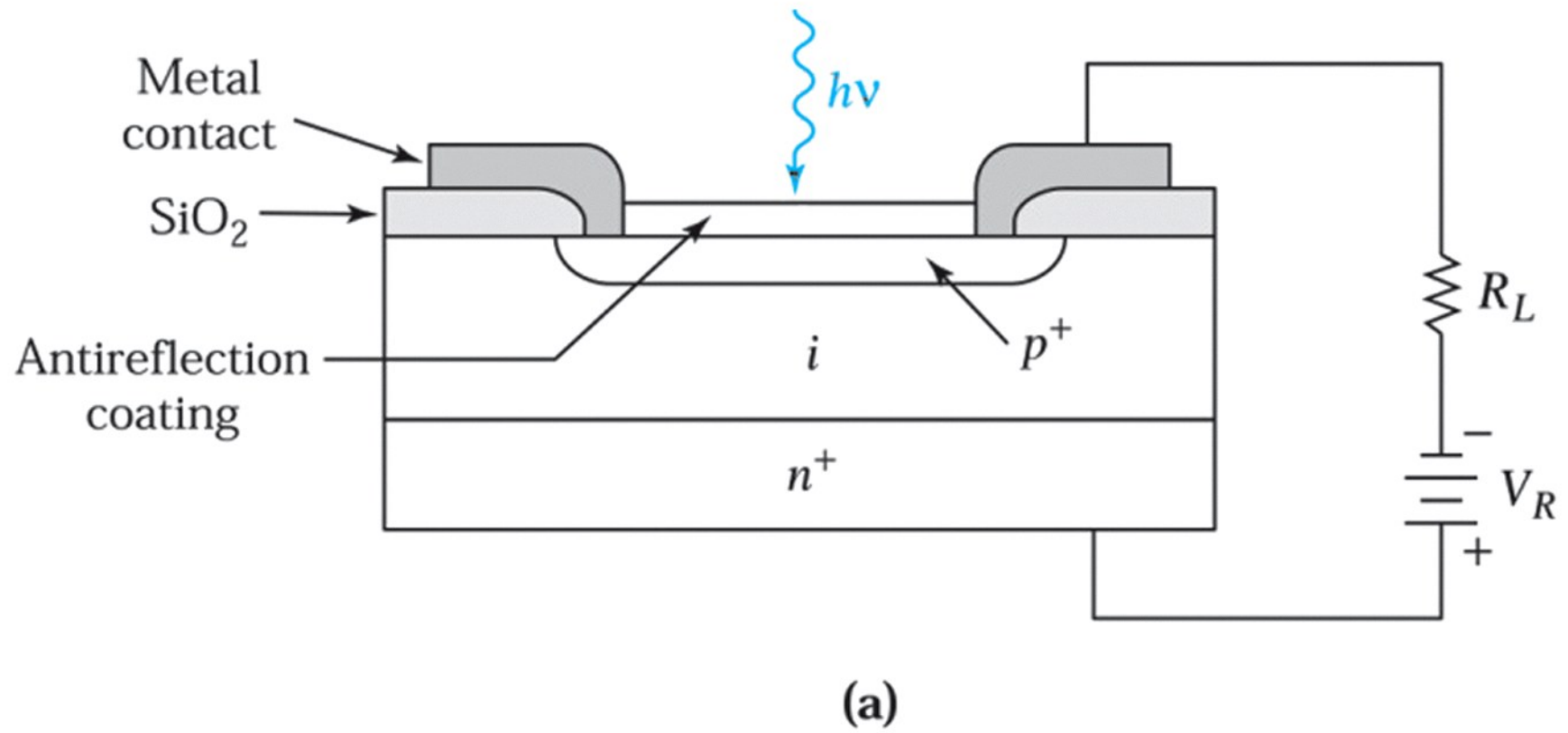
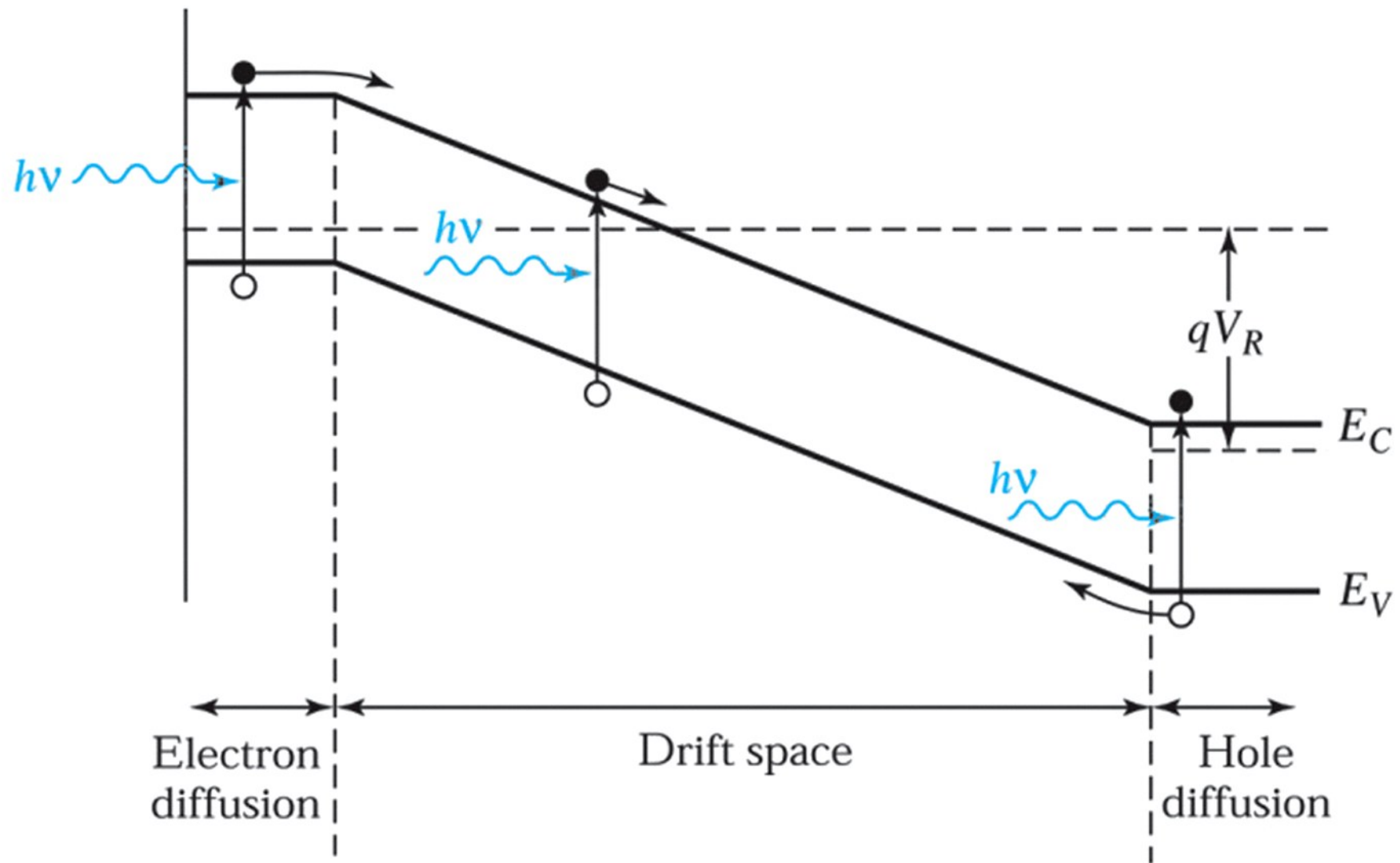


Figure 10.4a
© John Wiley & Sons, Inc. All rights reserved.



(b)

Figure 10.4b
 © John Wiley & Sons, Inc. All rights reserved.

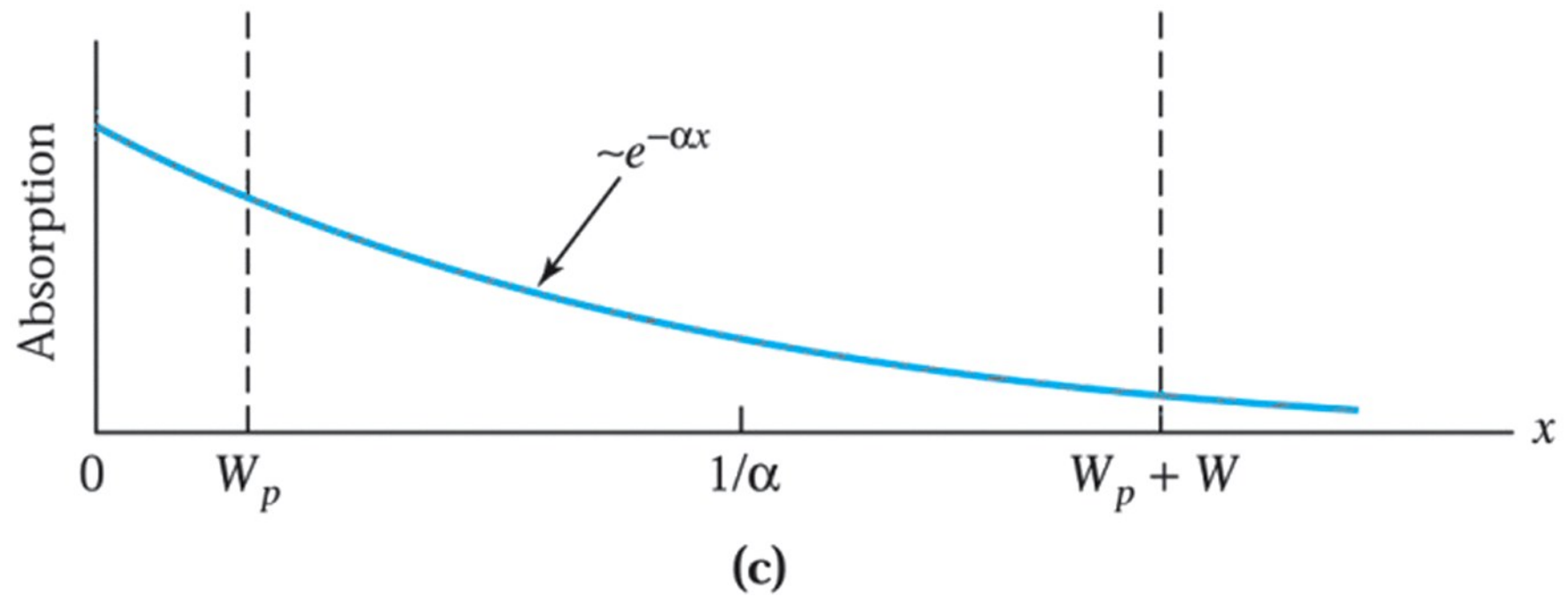
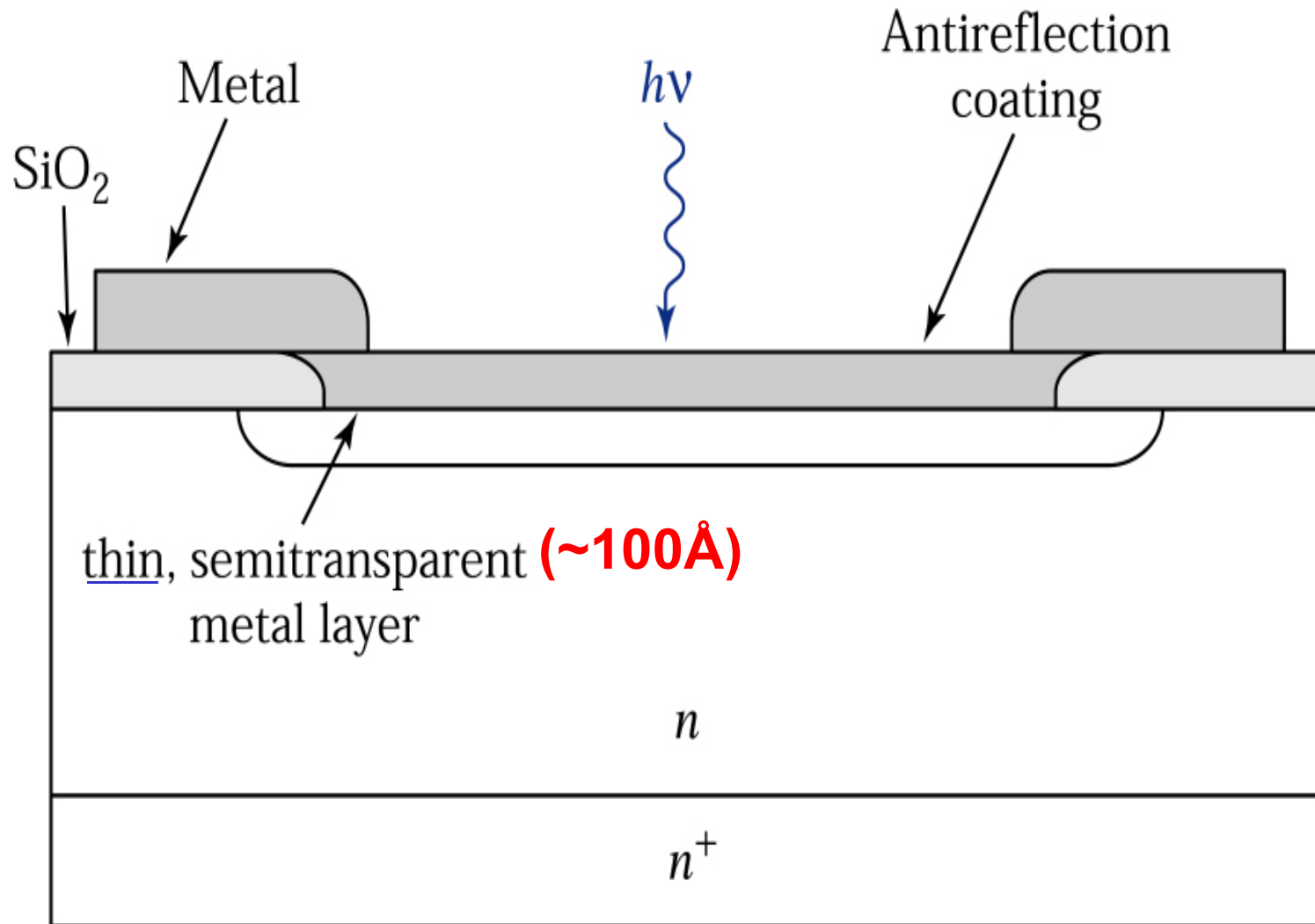
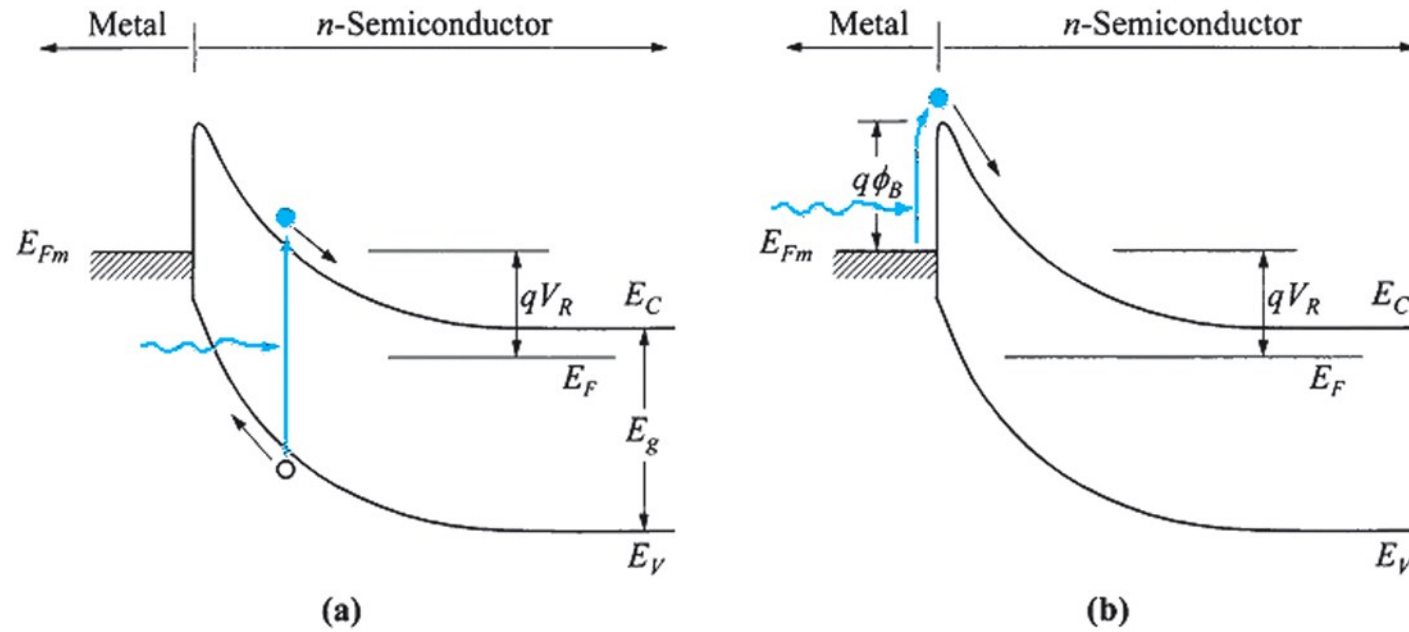


Figure 10.4c
© John Wiley & Sons, Inc. All rights reserved.



*沒有P+之吸收

Figure 10.5. Metal-semiconductor photodiode.



- (a) $h\nu > E_g$
- (b) $q\Phi_B < h\nu < E_g$
- (c) Both processes

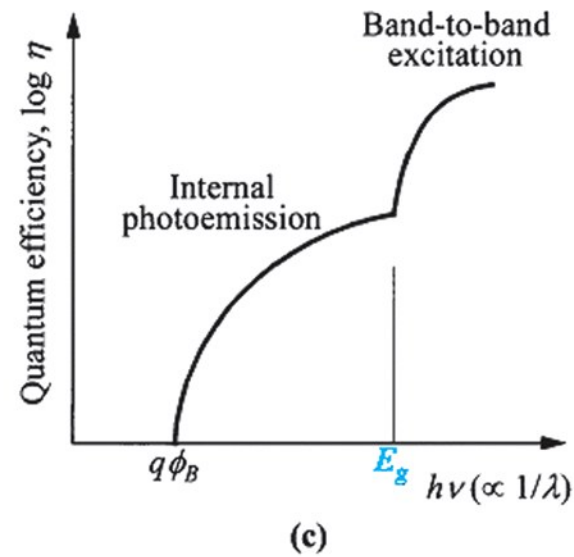


Figure 10.6
 © John Wiley & Sons, Inc. All rights reserved.

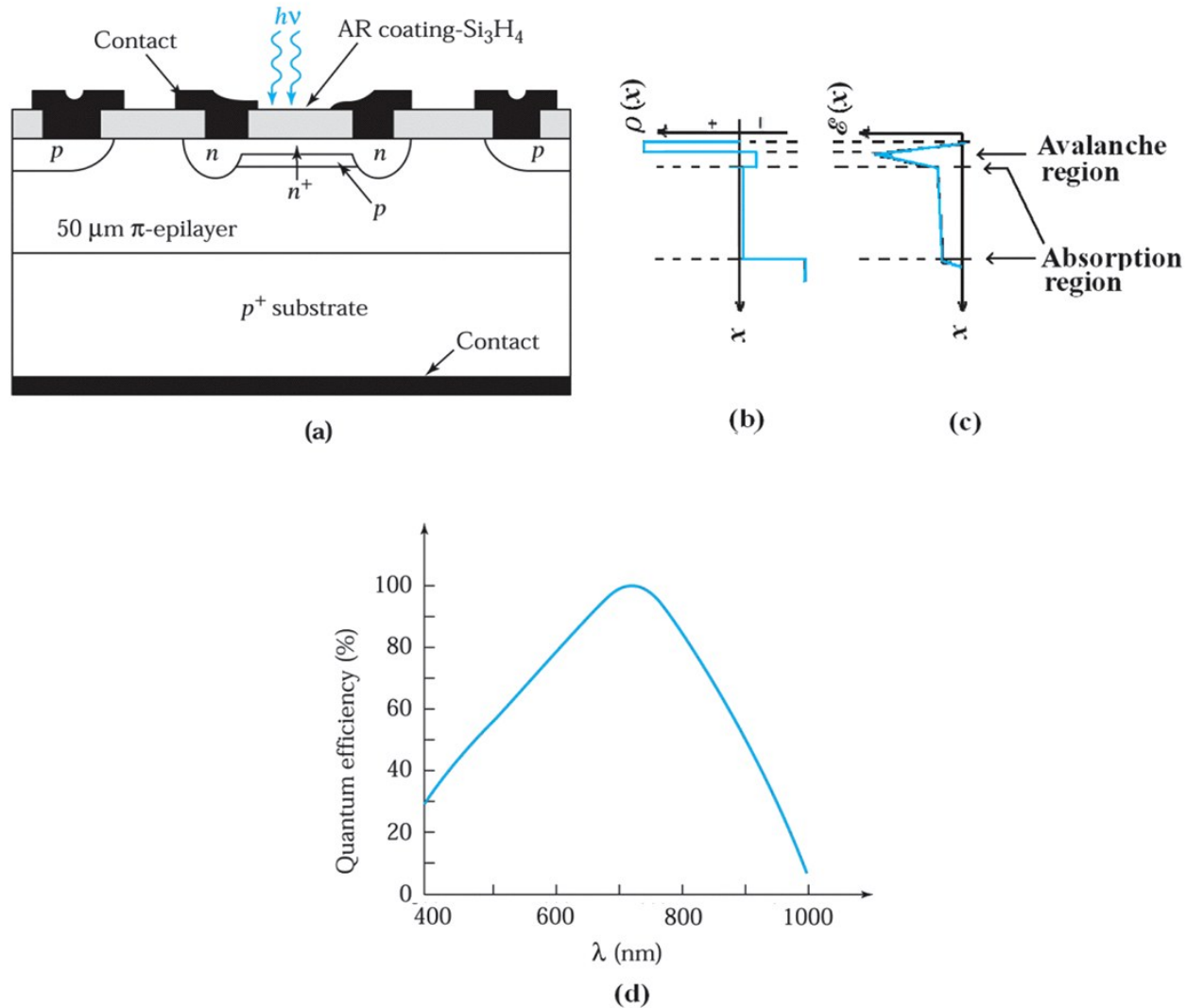
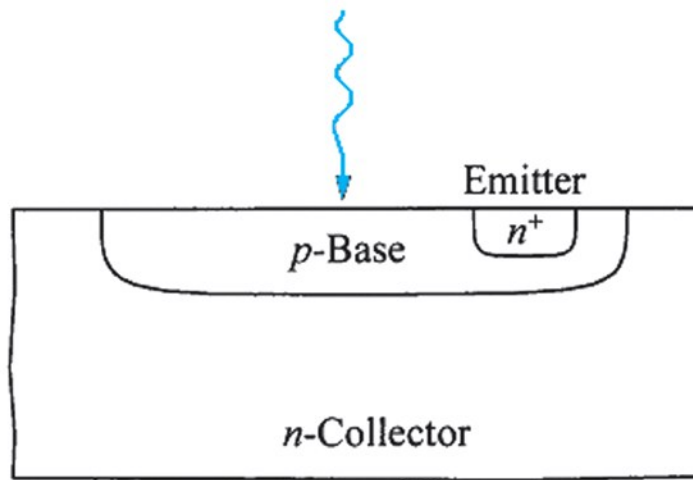


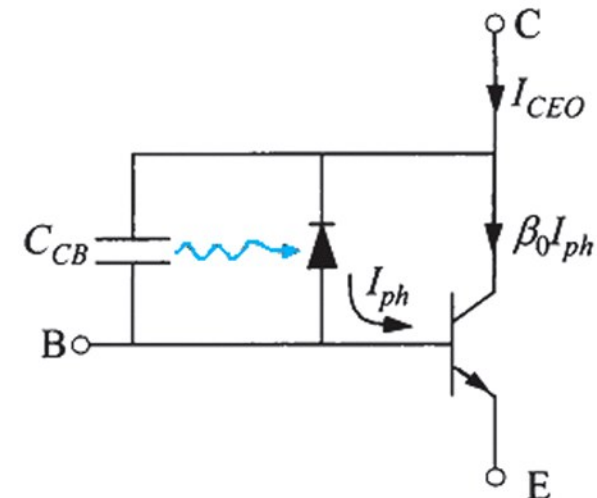
Figure 10.7.

A typical silicon **avalanche photodiode**: (a) device structure and (b) space charge (c) electric field (d) quantum efficiency.

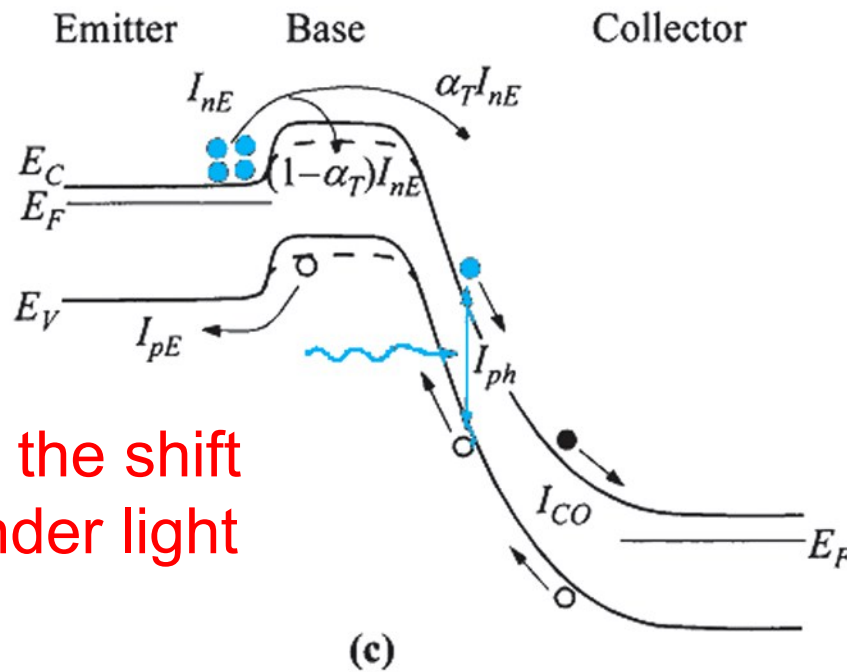
Avalanche: carrier 放大, 要避免 leakage, breakdown



(a)



(b)



(c)

Photo-transistor
(c) dash line shows the shift
of base potential under light

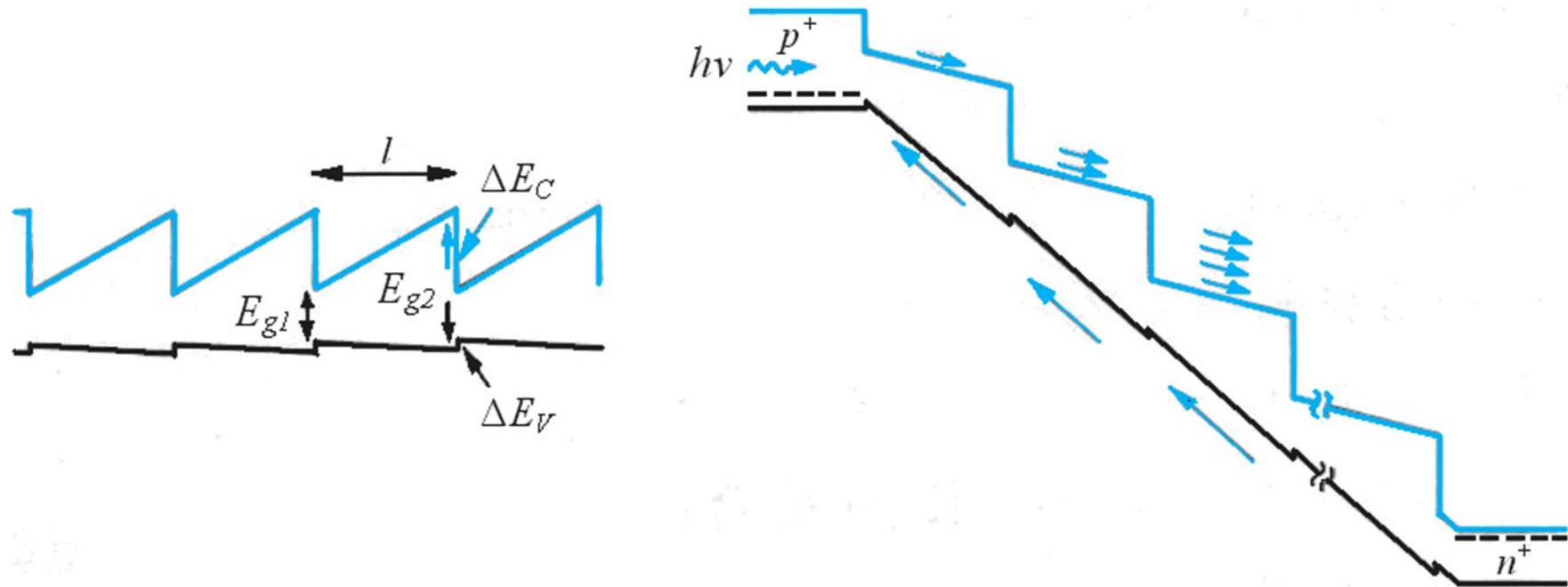


Figure 10.9

Reprinted with permission from *Applied Physics Letters*, 40 (38), F. Capasso et. al, "Enchantment of Electron Impact Ionisation in a Superlattice: A New Avalanche Photodiode with a Large Ionisation Rate Ratio", Copyright 1982 American Institute of Physics.

A staircase superlattice APD
 No high E, low noise

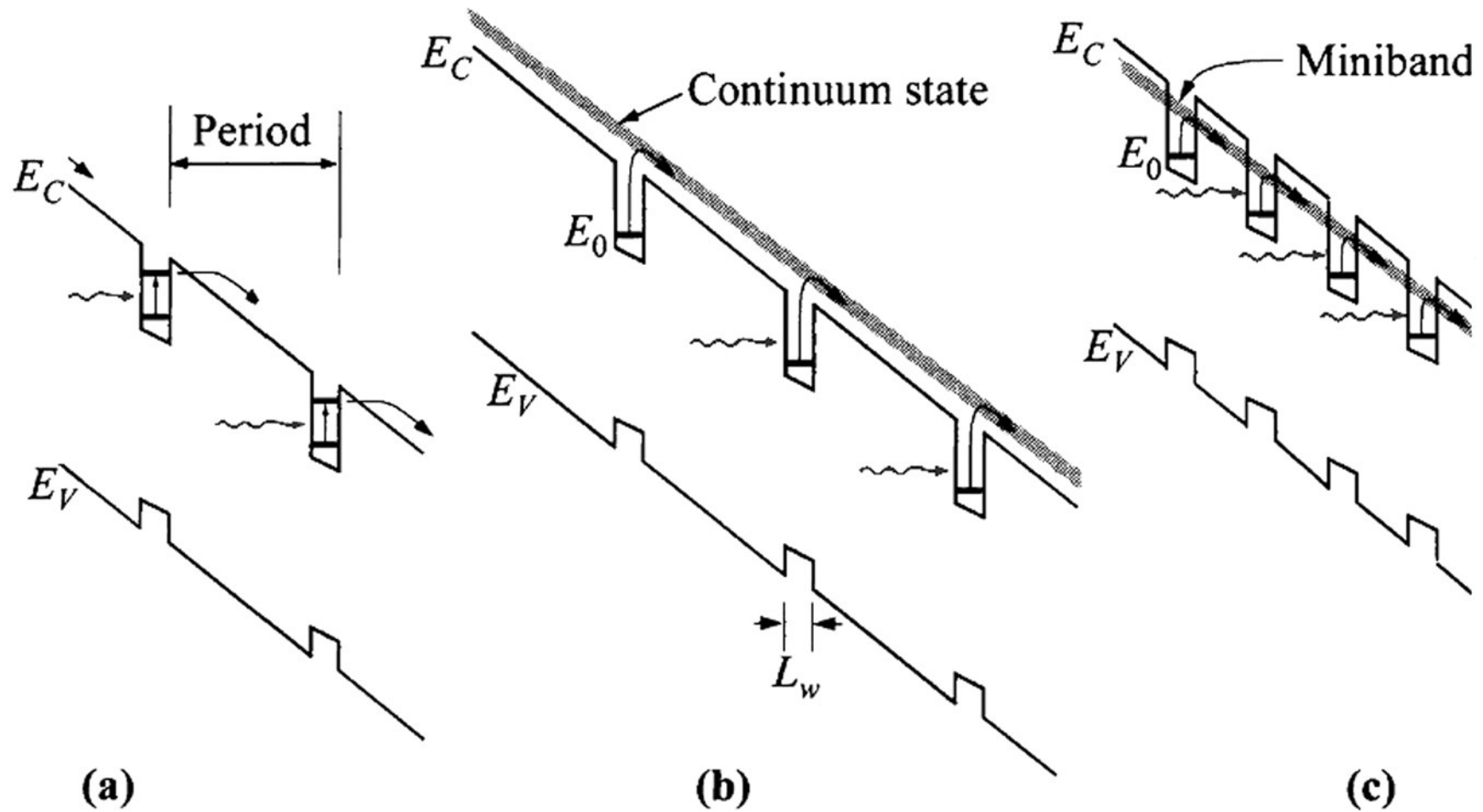
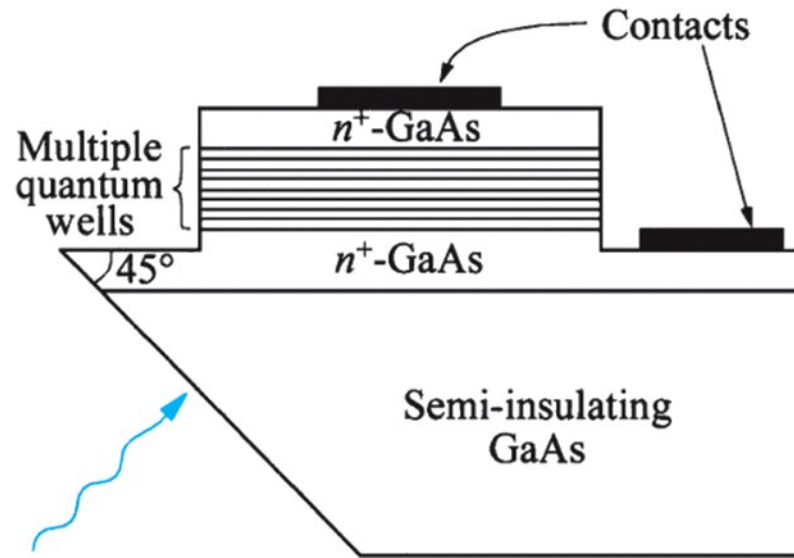
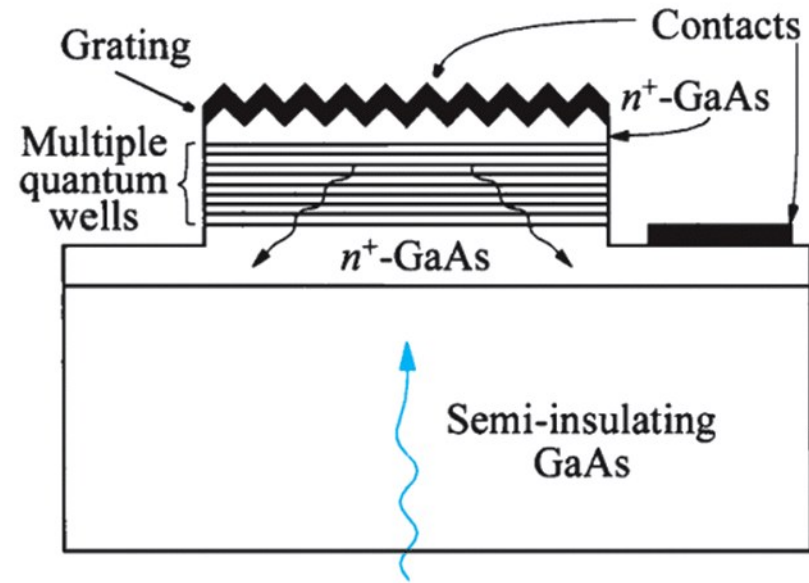


Figure 10.10
 © John Wiley & Sons, Inc. All rights reserved.

A quantum-well infrared photodetector (QWIP)



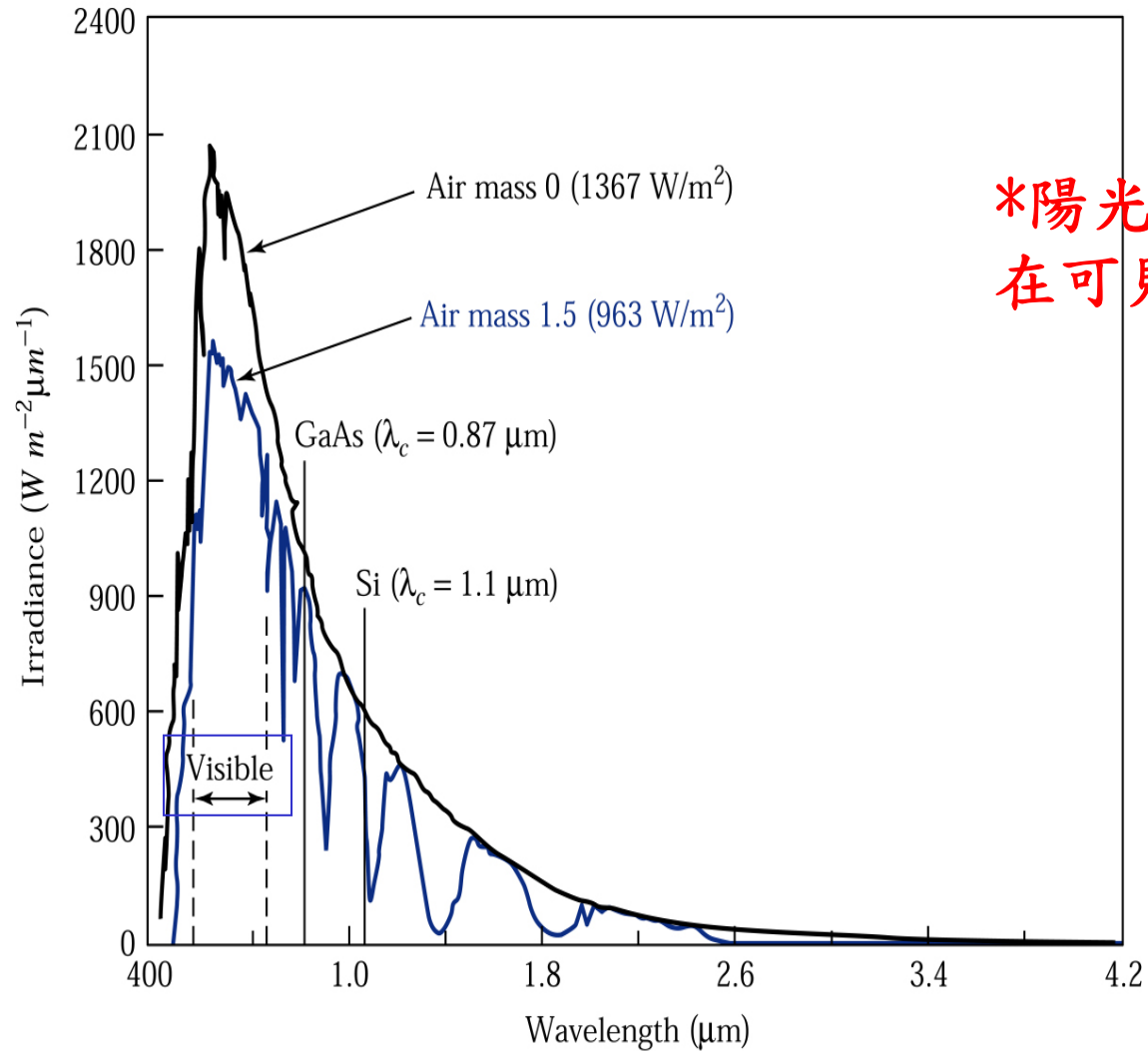
(a)



(b)

Figure 10.11
 © John Wiley & Sons, Inc. All rights reserved.

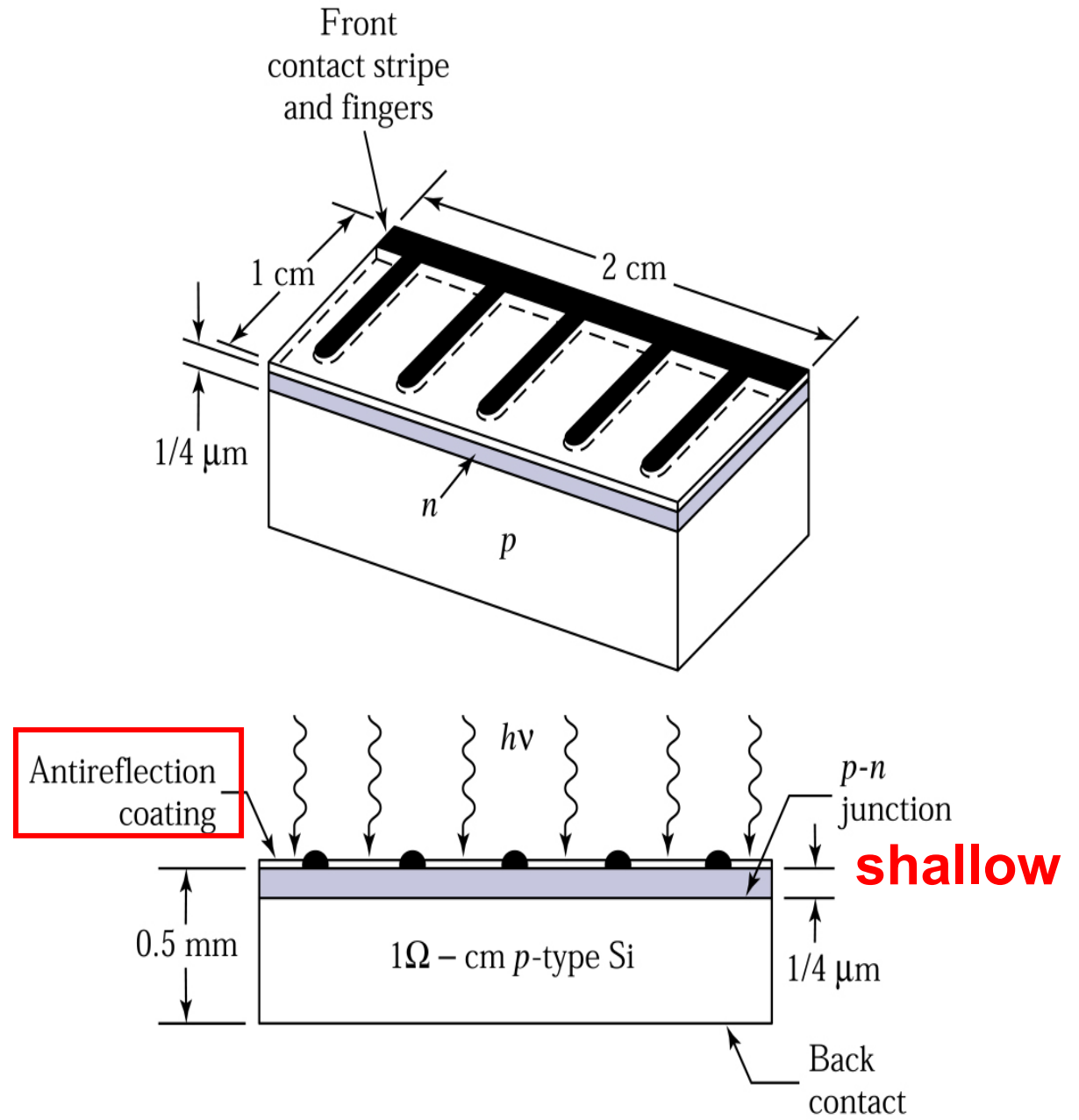
- (a) Light normal to 45° face, transparent to substrate
- (b) Grating on the top



*陽光中主要能量
在可見光

Figure 10.12. Solar **spectral irradiance**²⁵ at air mass 0 and air mass 1.5 and the cutoff wavelength of GaAs and Si.

Figure 10.13.
Schematic
representation of a
silicon *p-n* junction
solar cell.²³



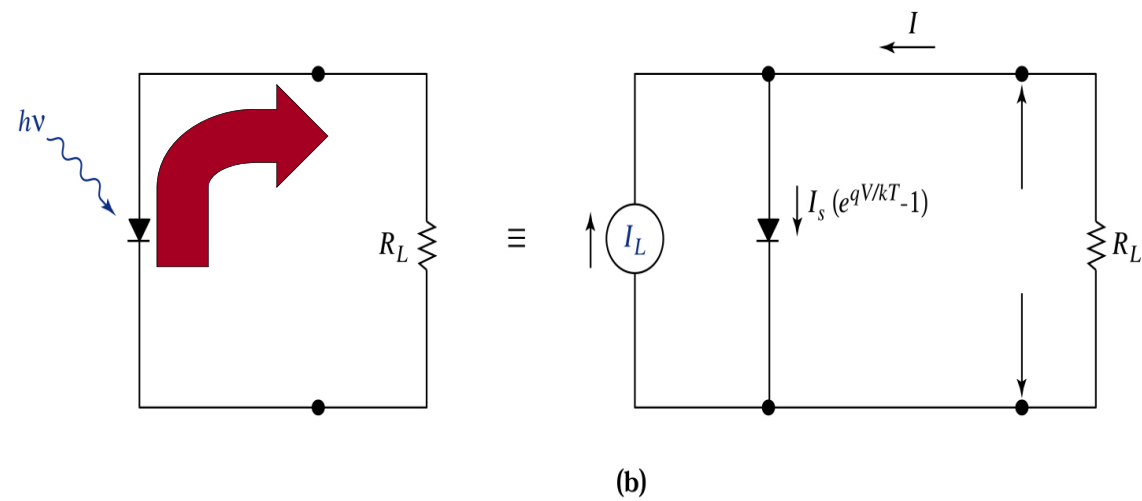
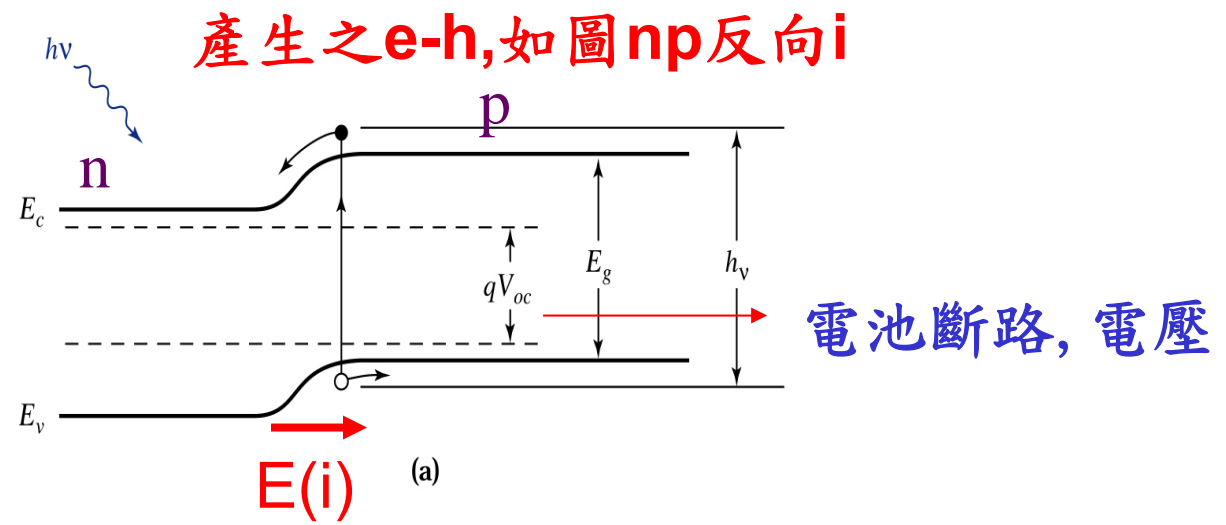


Figure 10.14. (a) Energy band diagram of a p - n junction solar cell under solar irradiation. (b) Idealized equivalent circuit of a solar cell.

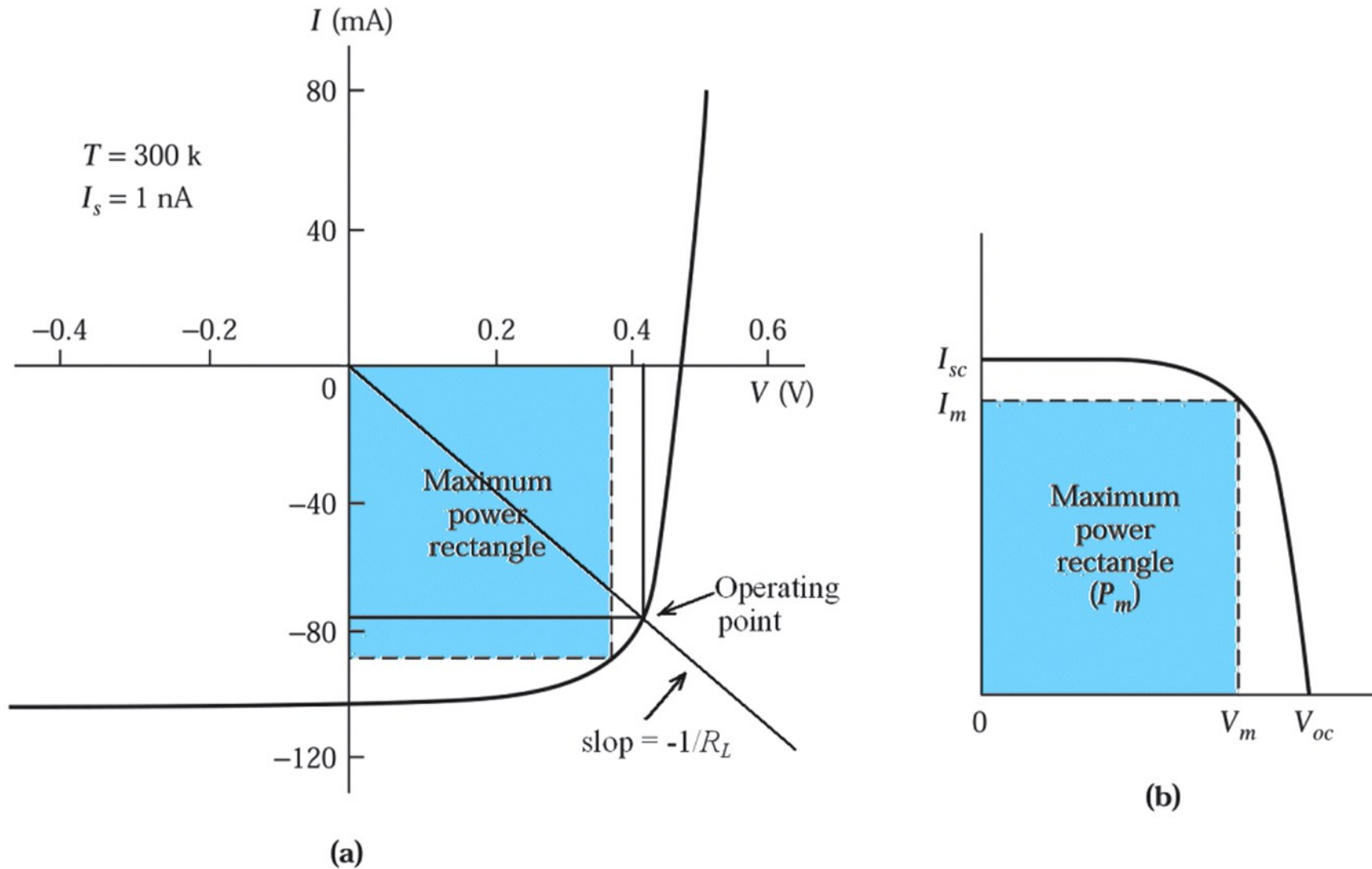
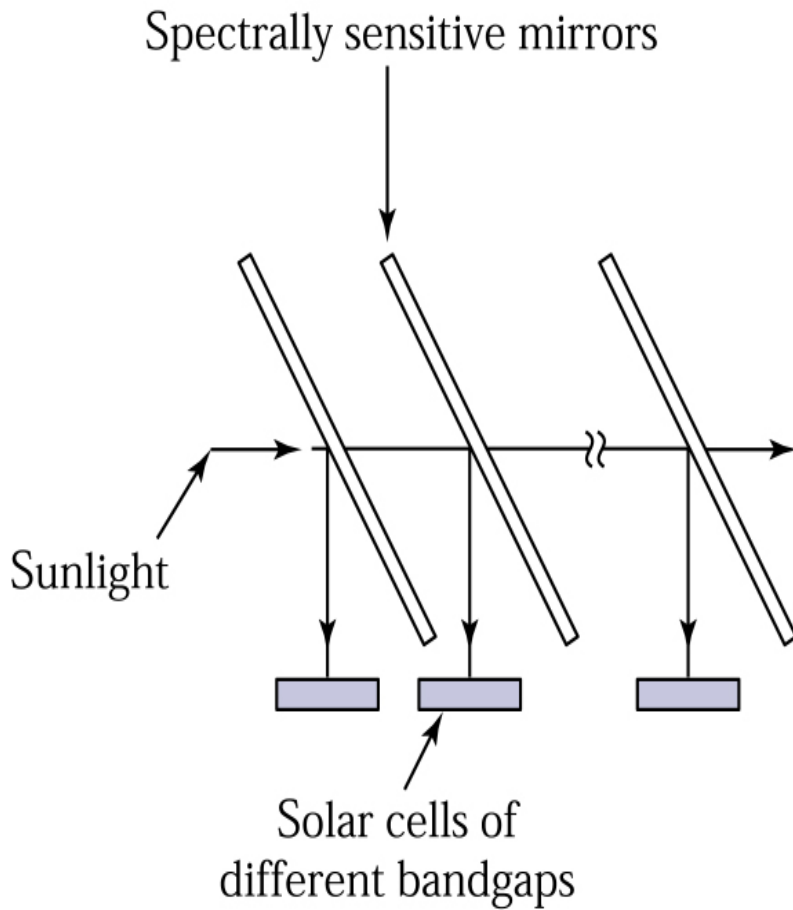


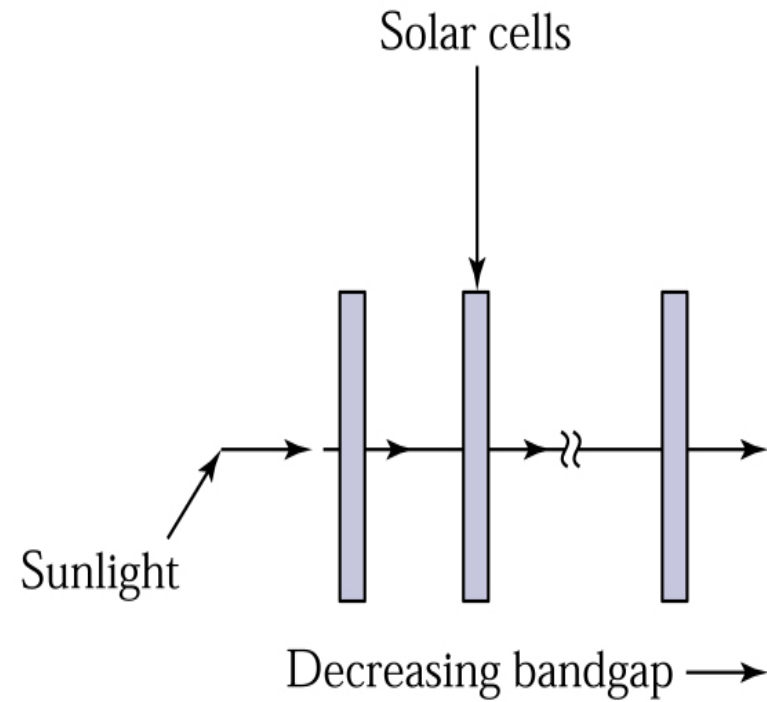
Figure 10.15

© John Wiley & Sons, Inc. All rights reserved.

Figure 10.15. (a) Current voltage characteristics of a solar cell under illumination. (b) Inversion of (a) about the voltage axis.



(a)



(b)

吸收更多波長

Figure 10.16. Multigap cell concepts. (a) Spectrum splitting approach. (b) **Tandem-cell** approach.²⁷

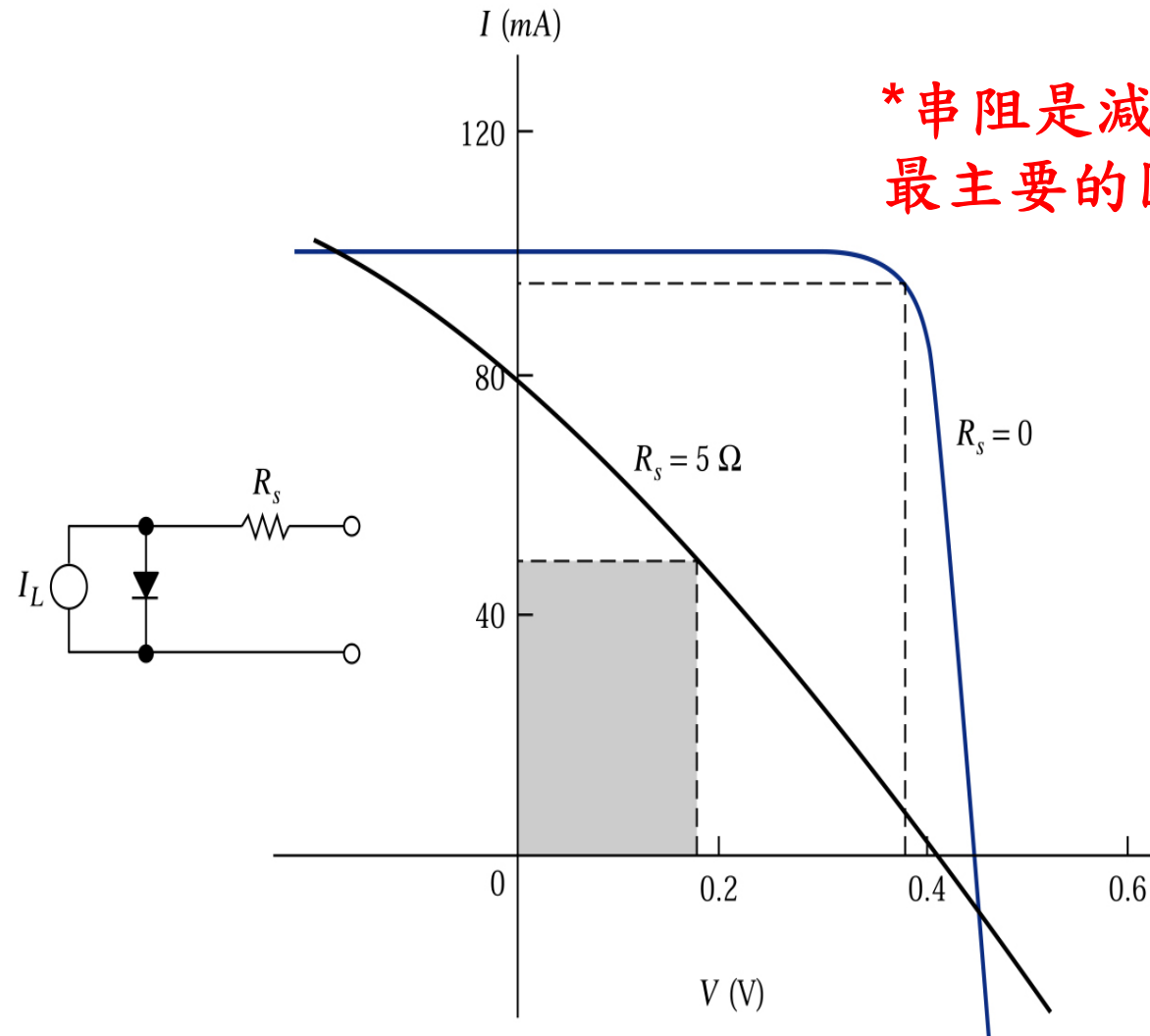


Figure 10.17. Current-voltage characteristics and the equivalent circuit of solar cells that have resistances.

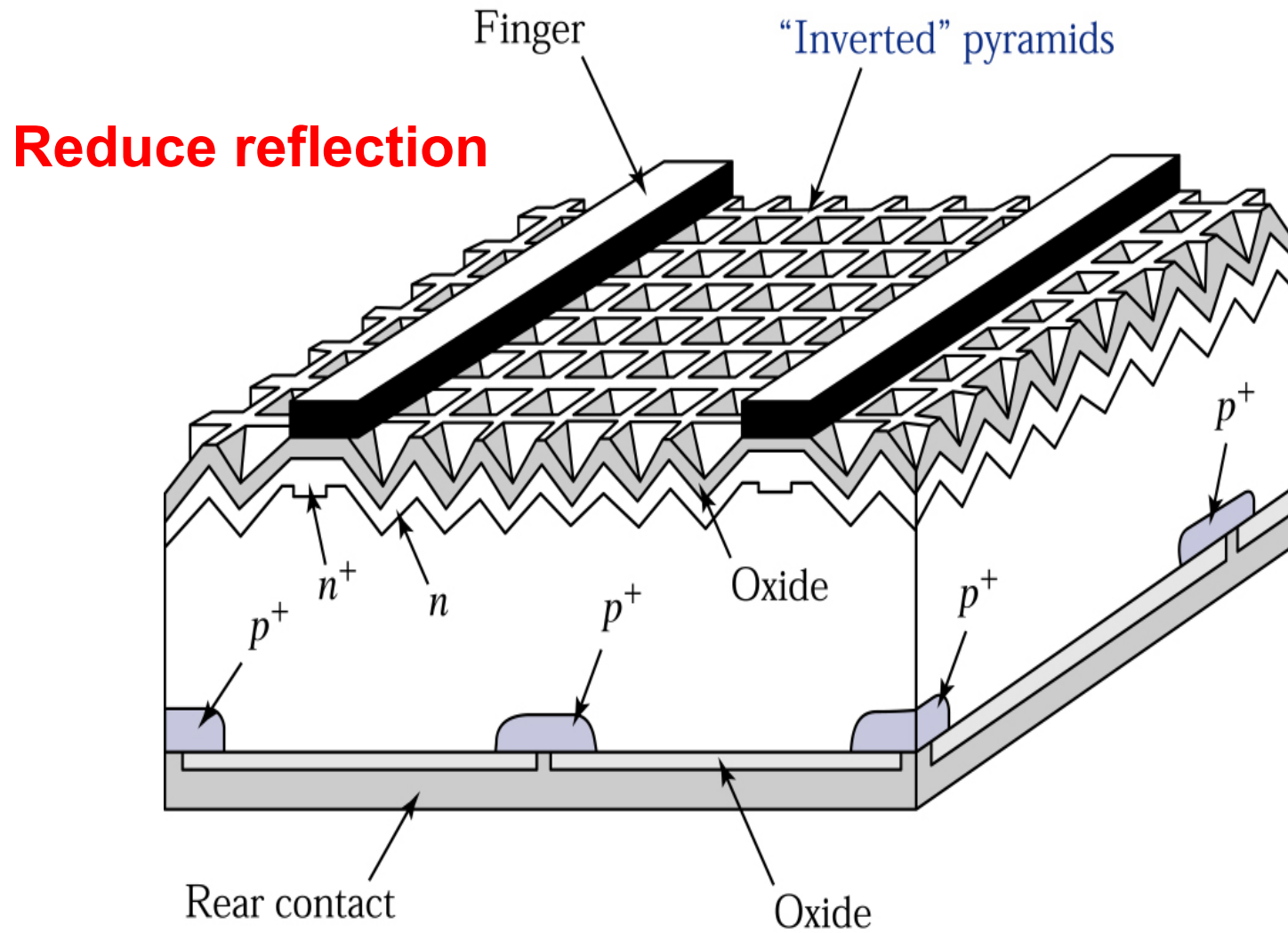


Figure 10.18a. Passivated emitter rear locally diffused (PERL) cell.²⁴

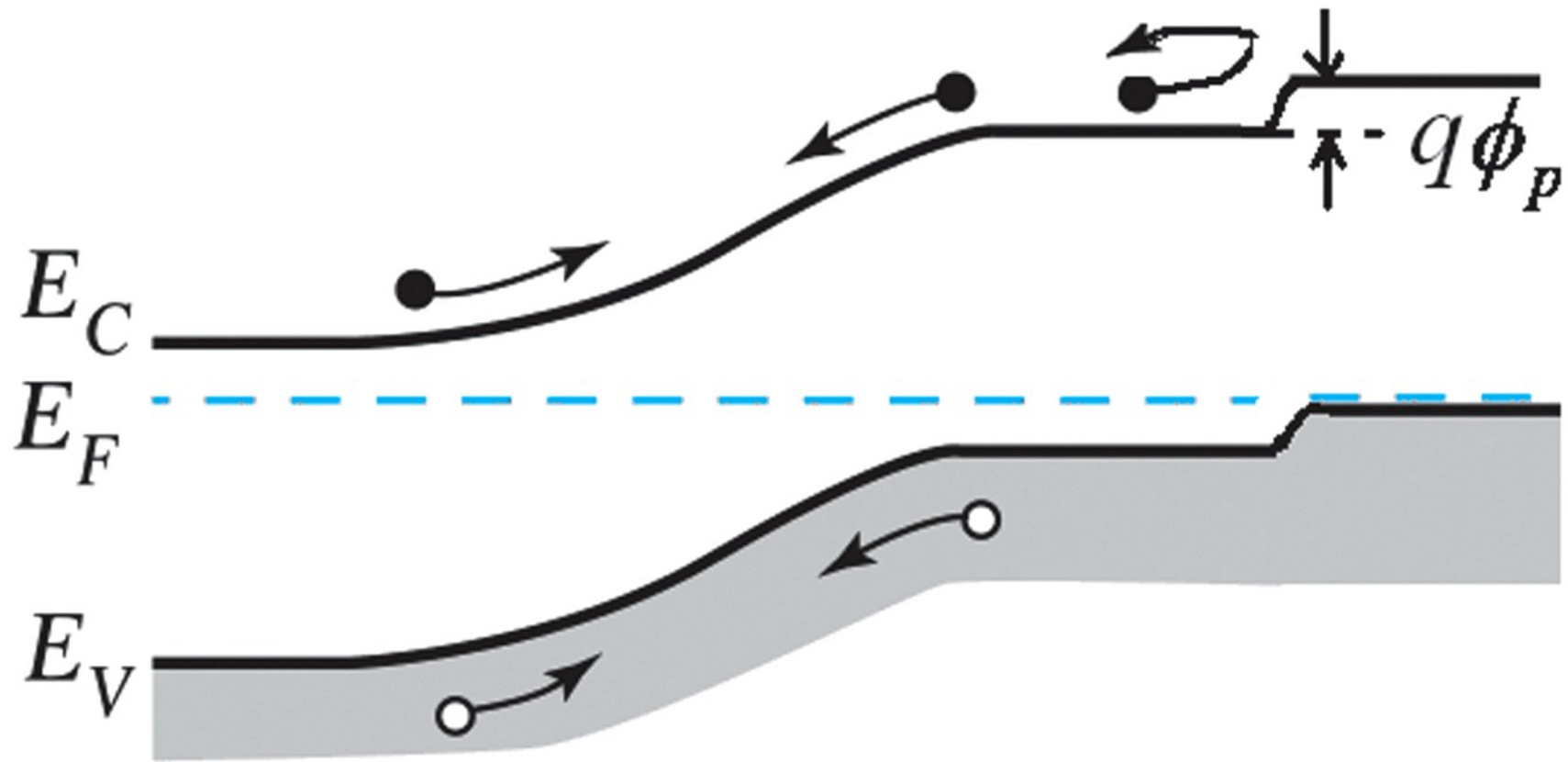
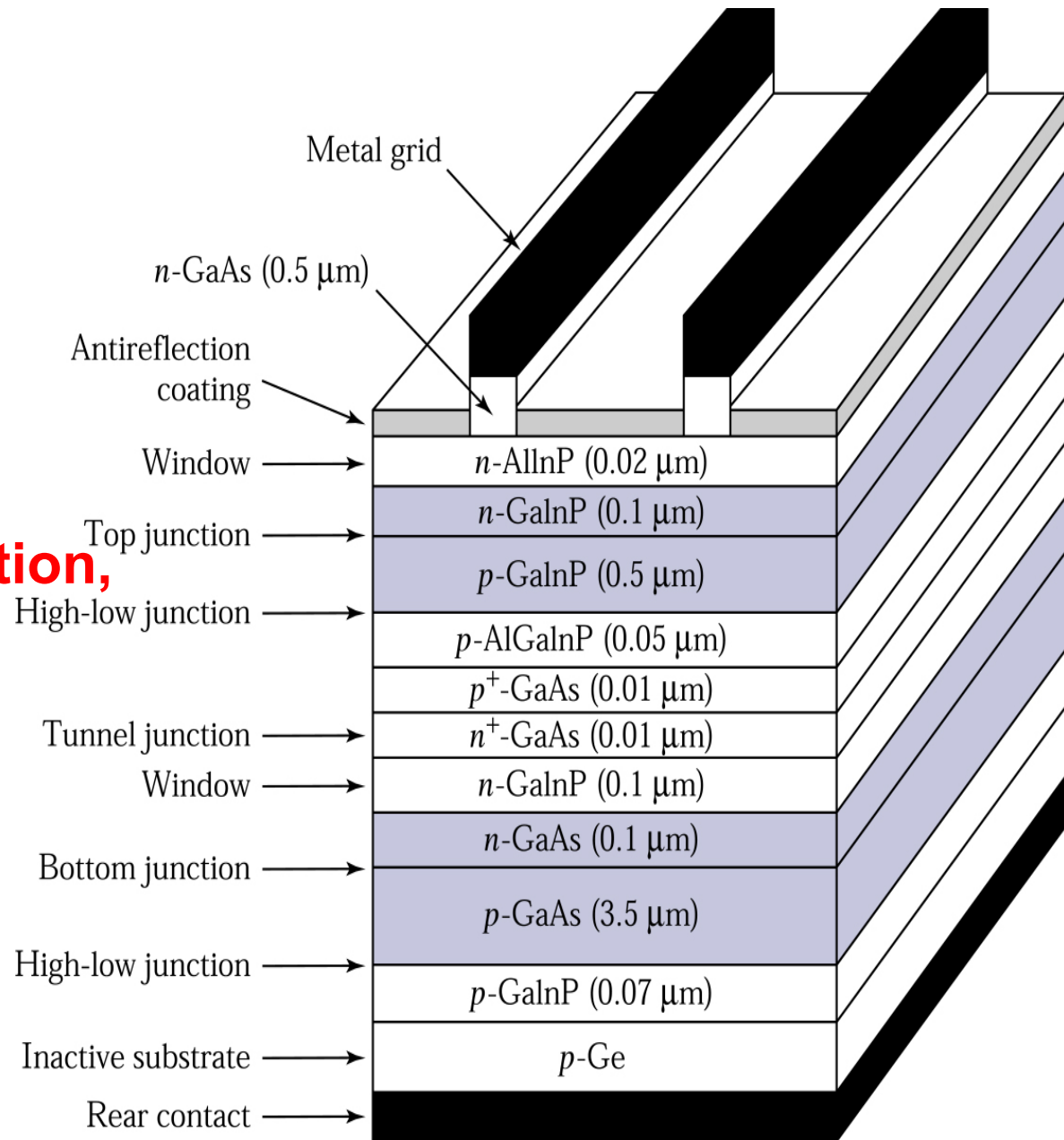


Figure 10.18b
 © John Wiley & Sons, Inc. All rights reserved.

Back-surface field

Figure 10.19.
Monolithic tandem
solar cell.²⁴

**Reduce recombination,
30% efficiency**



Lowest cost, 5% efficiency

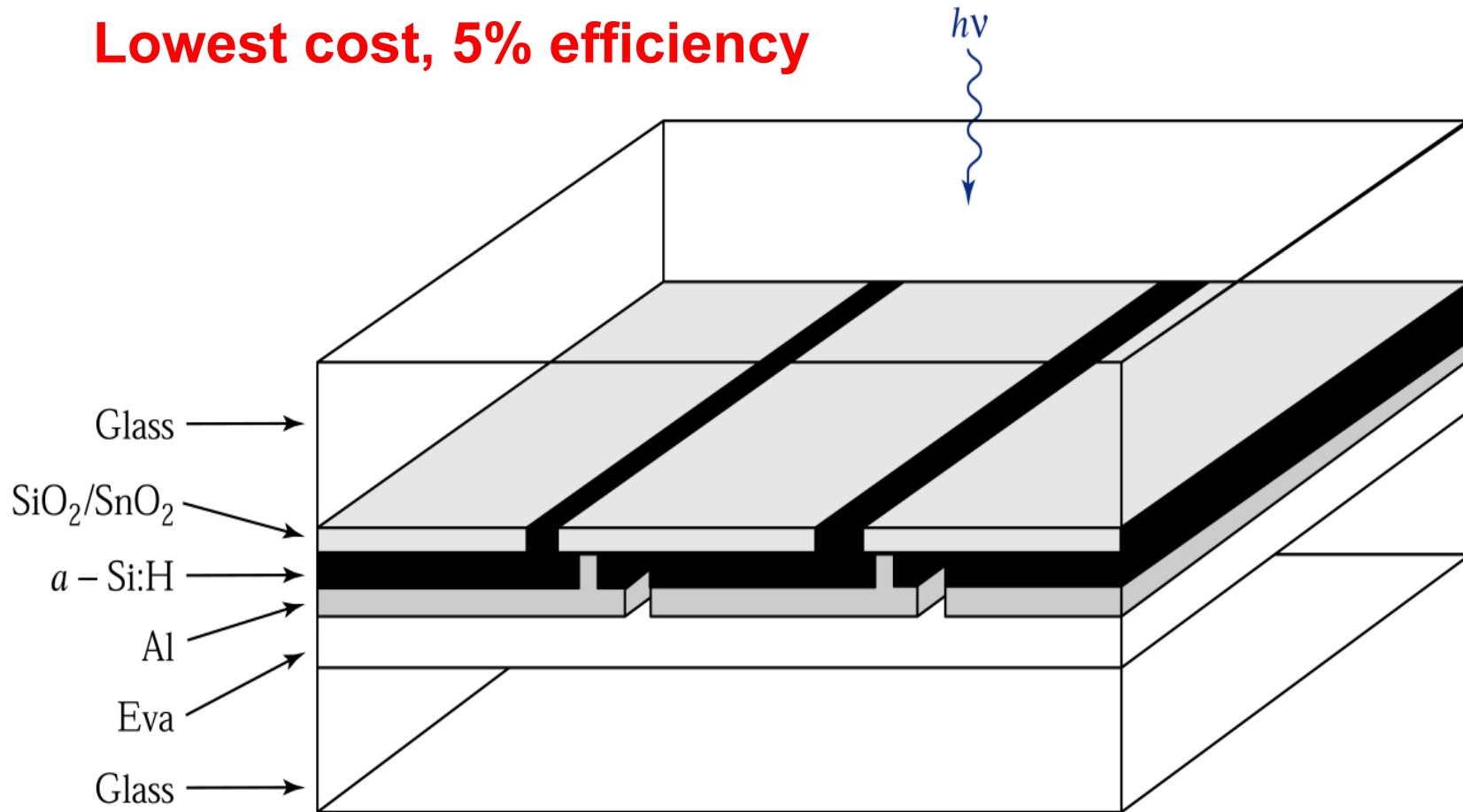


Figure 10.20. Series-interconnected a-Si solar cells deposited on a glass substrate with a rear glass cover bonded using ethylene vinyl acetate.

Micro-crystalline/
amorphous tandem cell

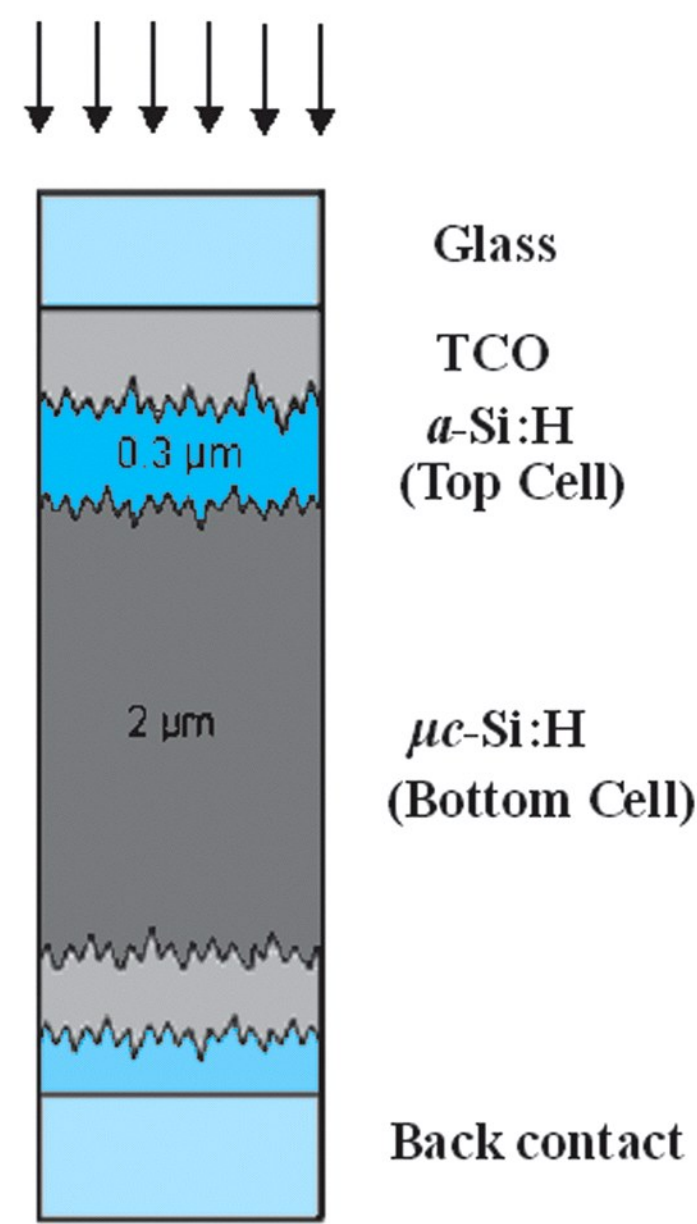


Figure 10.21a
Reprinted from *Solar Energy Materials and Solar Cells*, 78, A.V. Shah et. al, "Material and solar cell research in microcrystalline silicon", pp. 469-491, Copyright 2003, with permission from Elsevier.

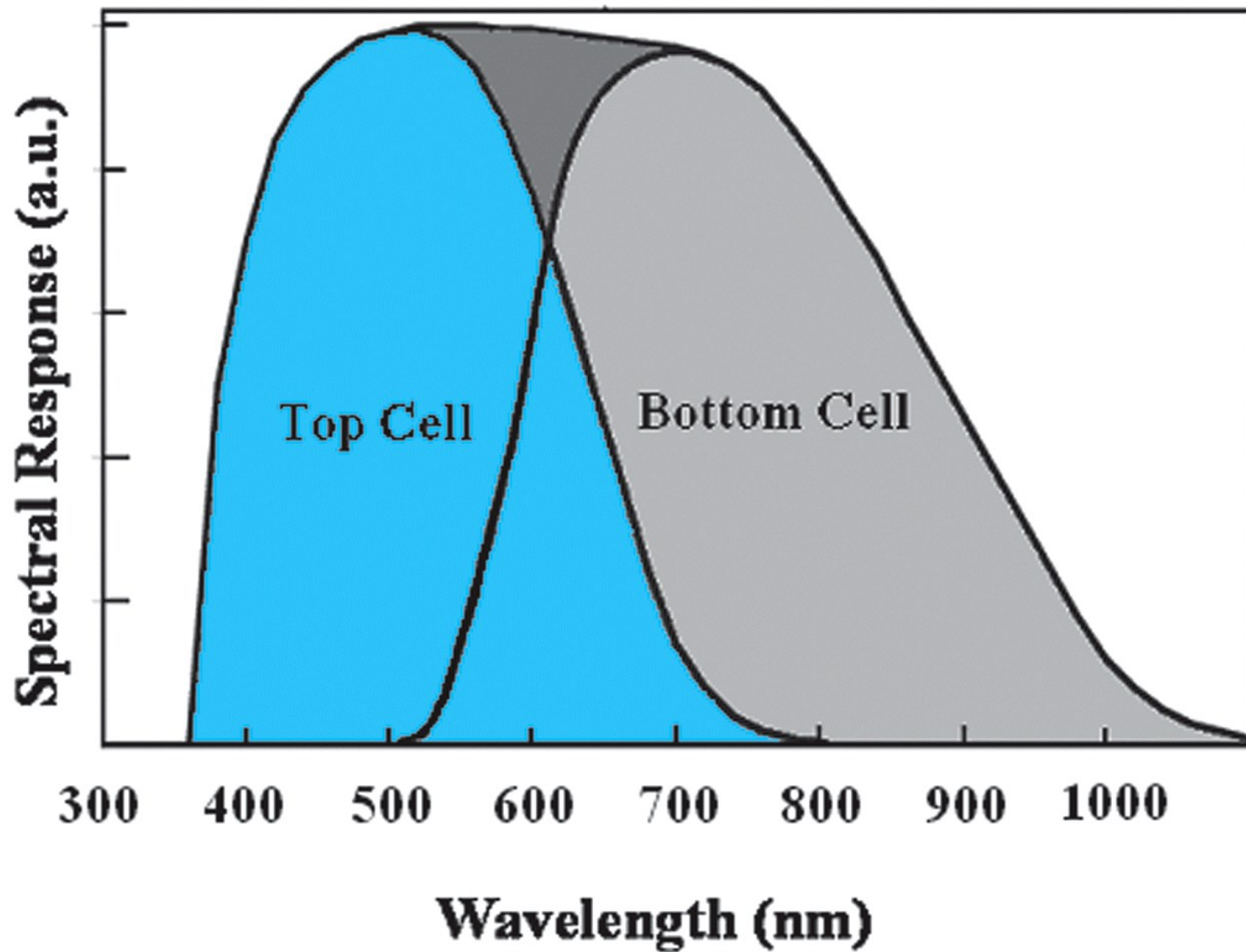


Figure 10.21b
Reprinted from *Solar Energy Materials and Solar Cells*, 78, A.V. Shah et. al, "Material and solar cell research in microcrystalline silicon", pp. 469-491, Copyright 2003, with permission from Elsevier.

Response of micro-crystalline/amorphous tandem cell

Absorption α of CuInSe_2

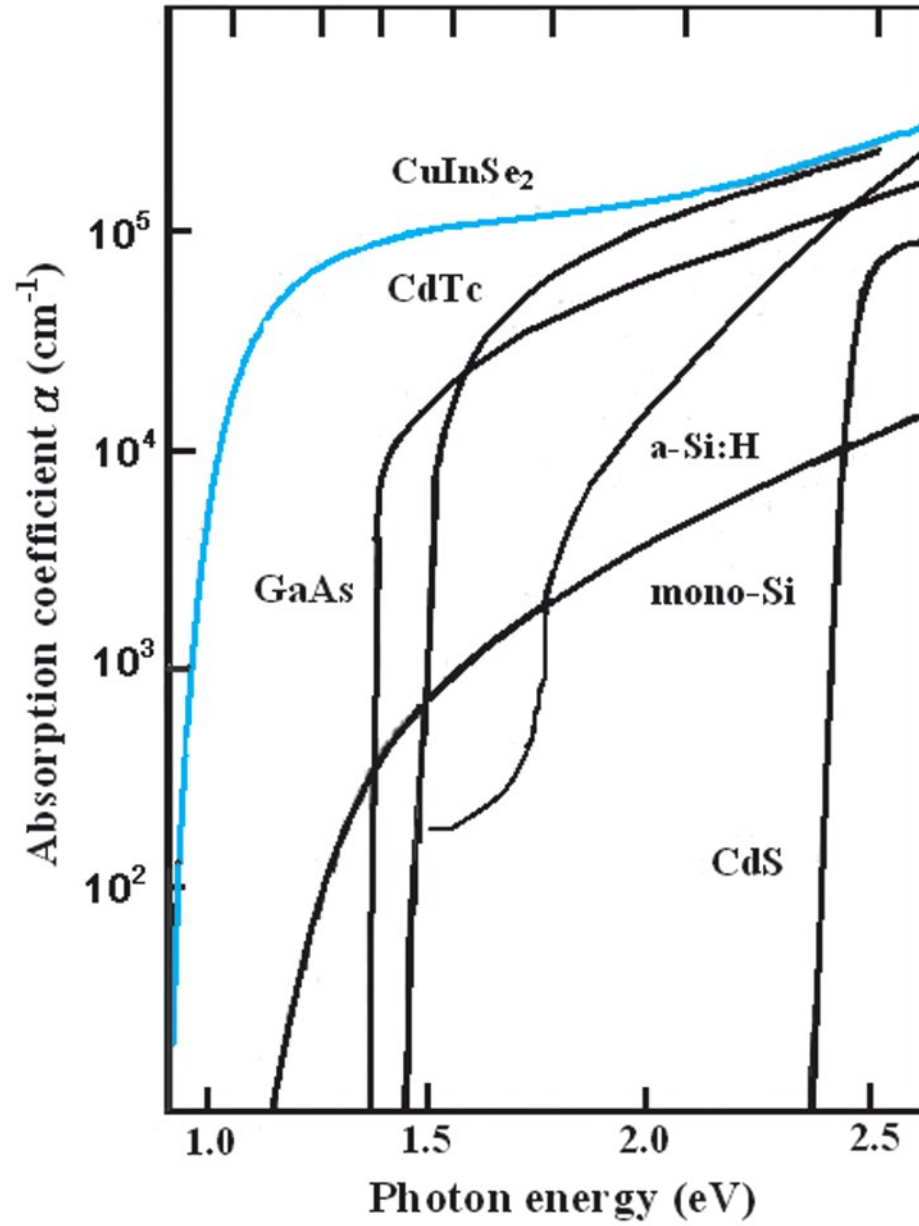


Figure 10.22a

© John Wiley & Sons, Inc. All rights reserved.

CIGS solar cell

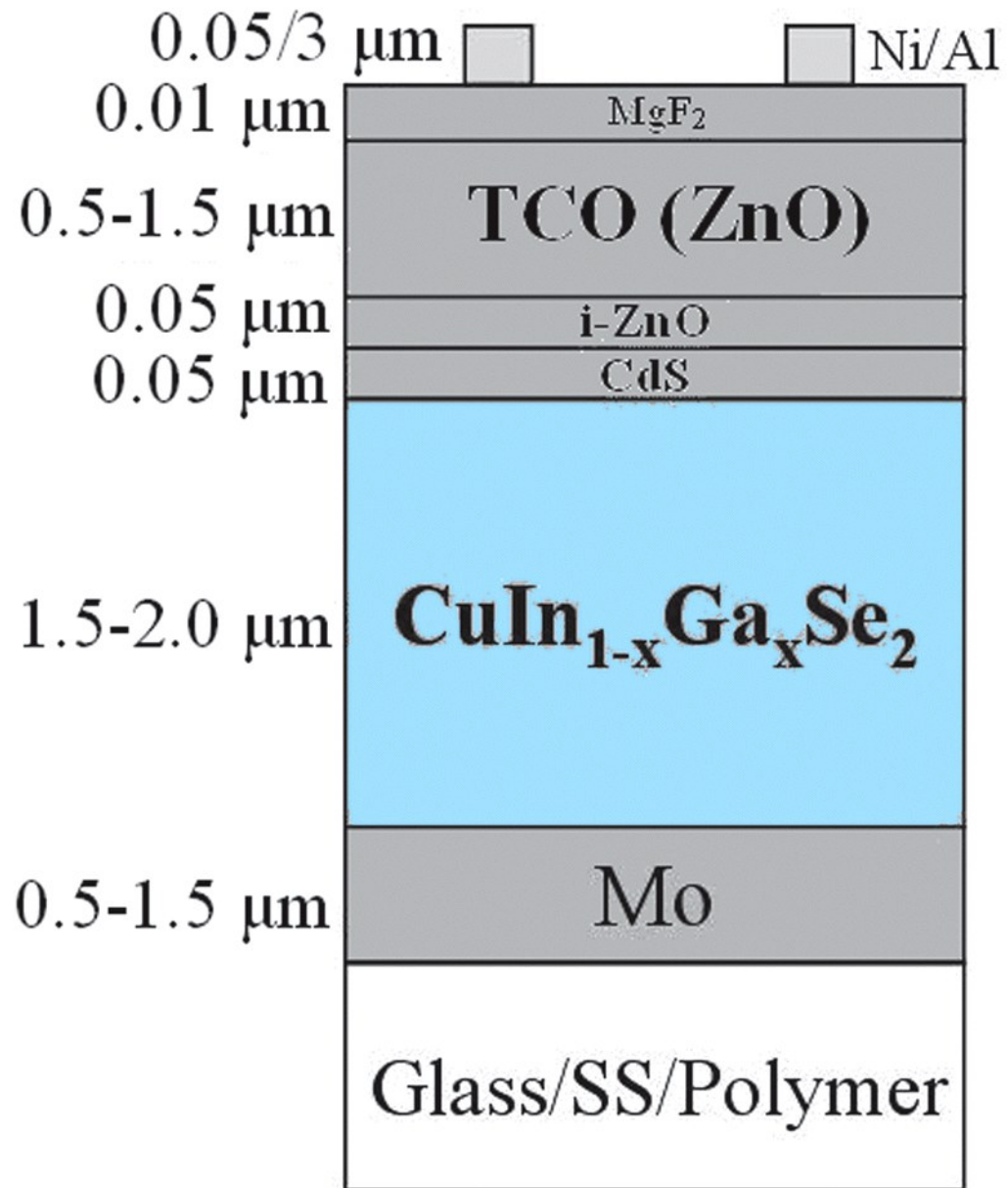


Figure 10.22b
© John Wiley & Sons, Inc. All rights reserved.

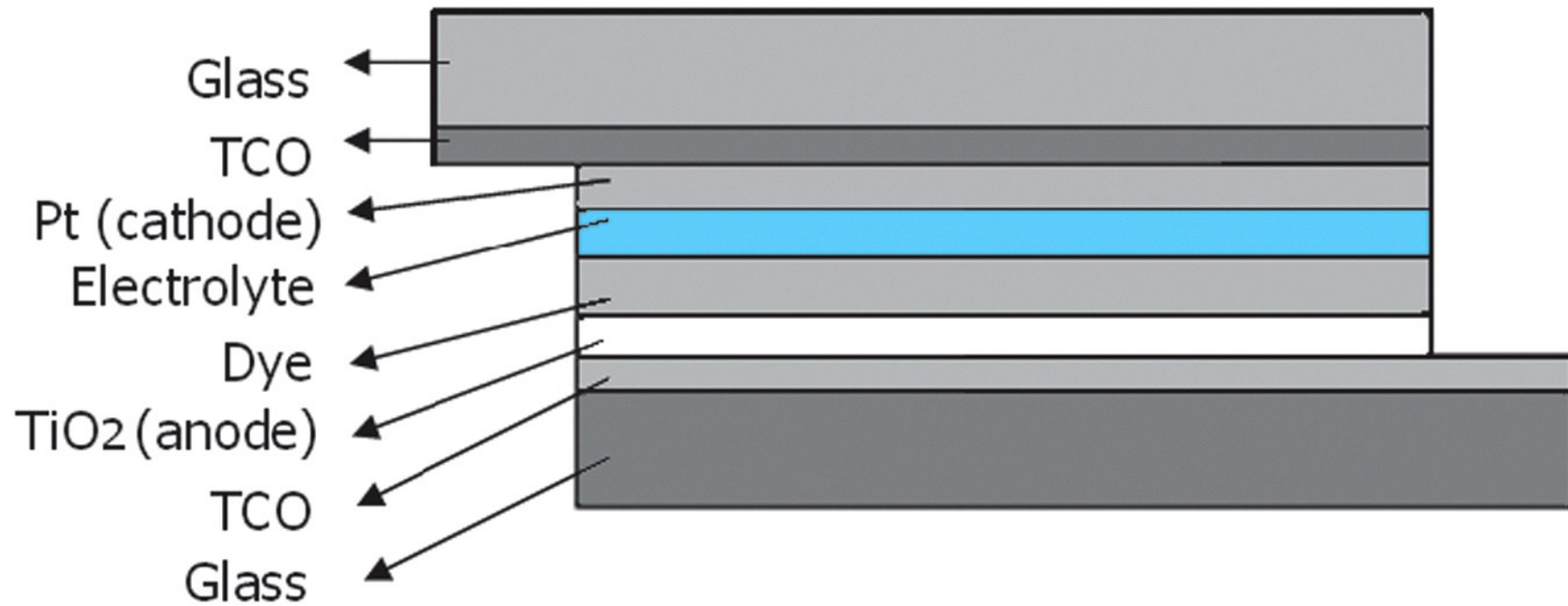


Figure 10.23a
© John Wiley & Sons, Inc. All rights reserved.

DSSC structure

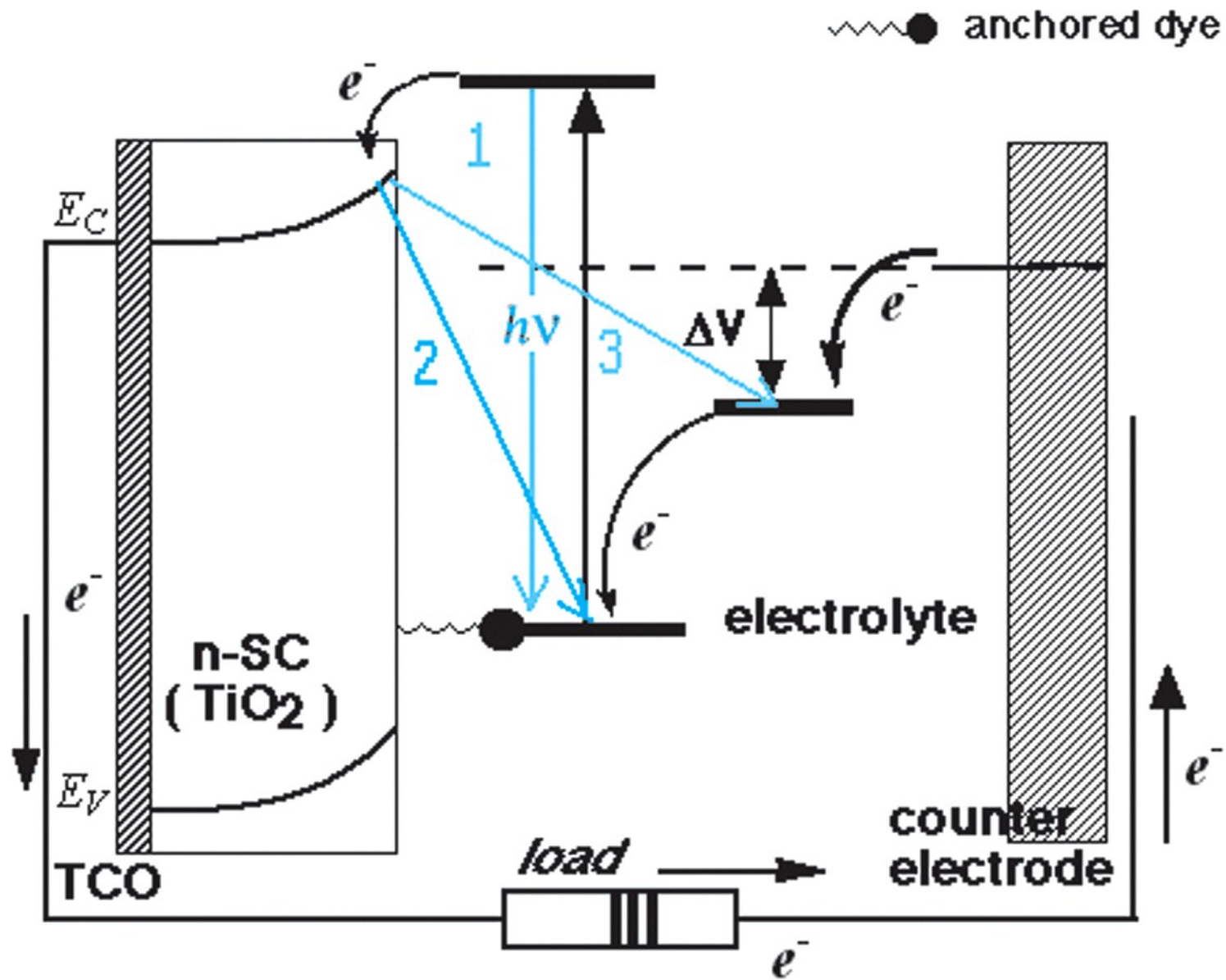


Figure 10.23b
 © John Wiley & Sons, Inc. All rights reserved.

DSSC band diagram and carrier losses

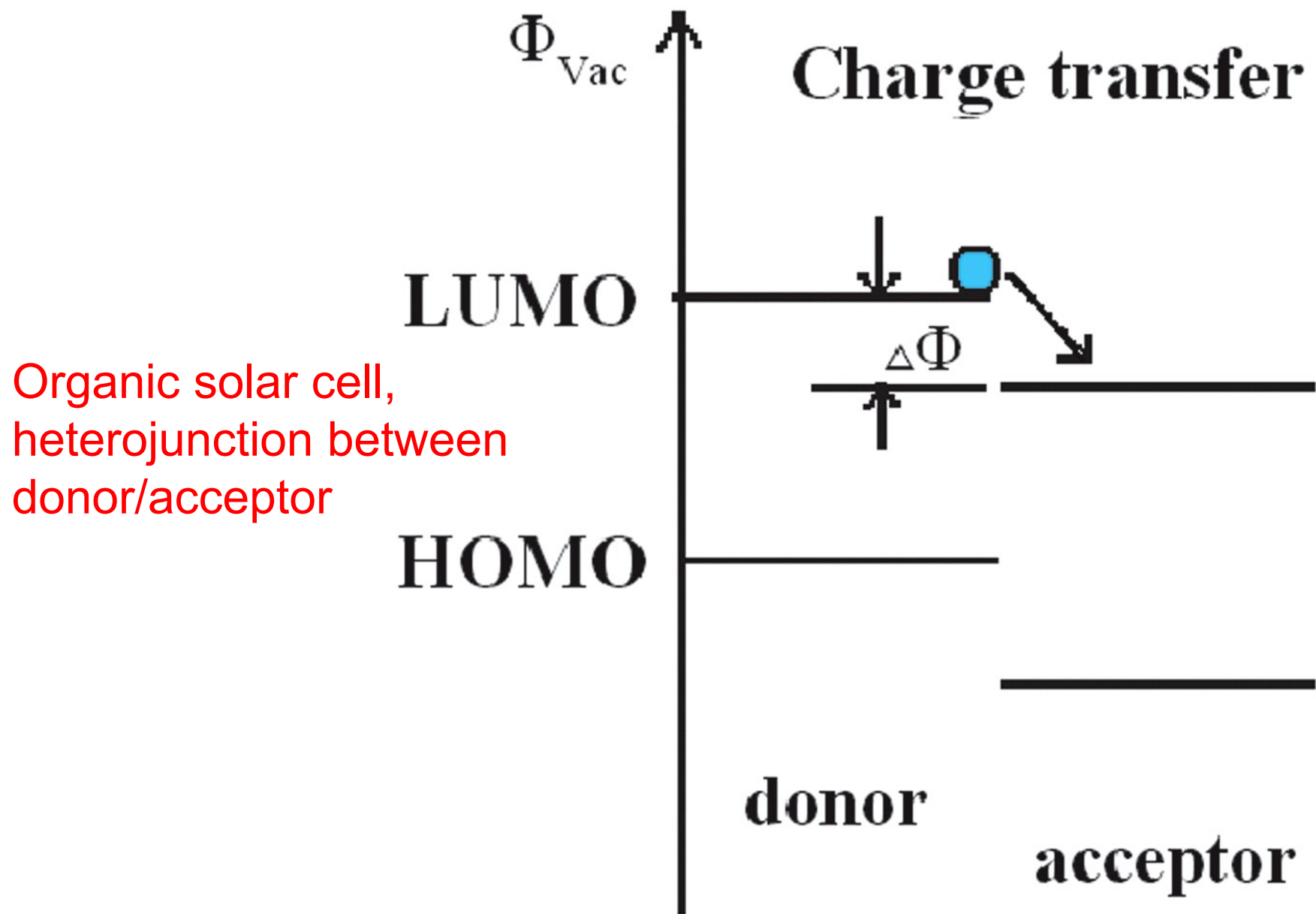


Figure 10.24
© John Wiley & Sons, Inc. All rights reserved.

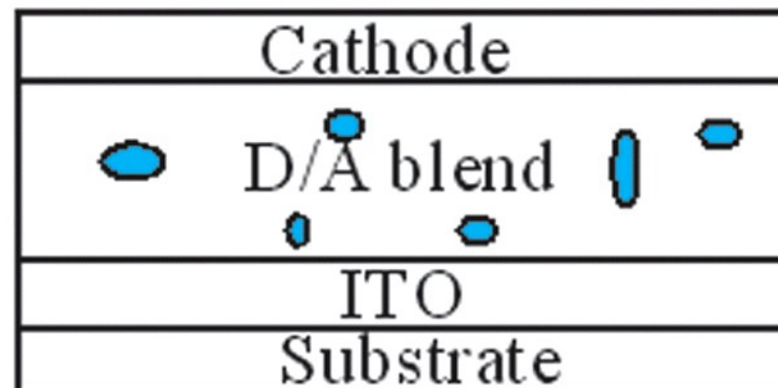
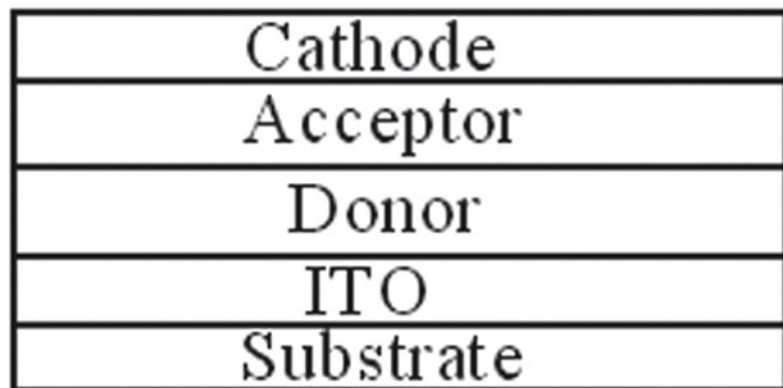
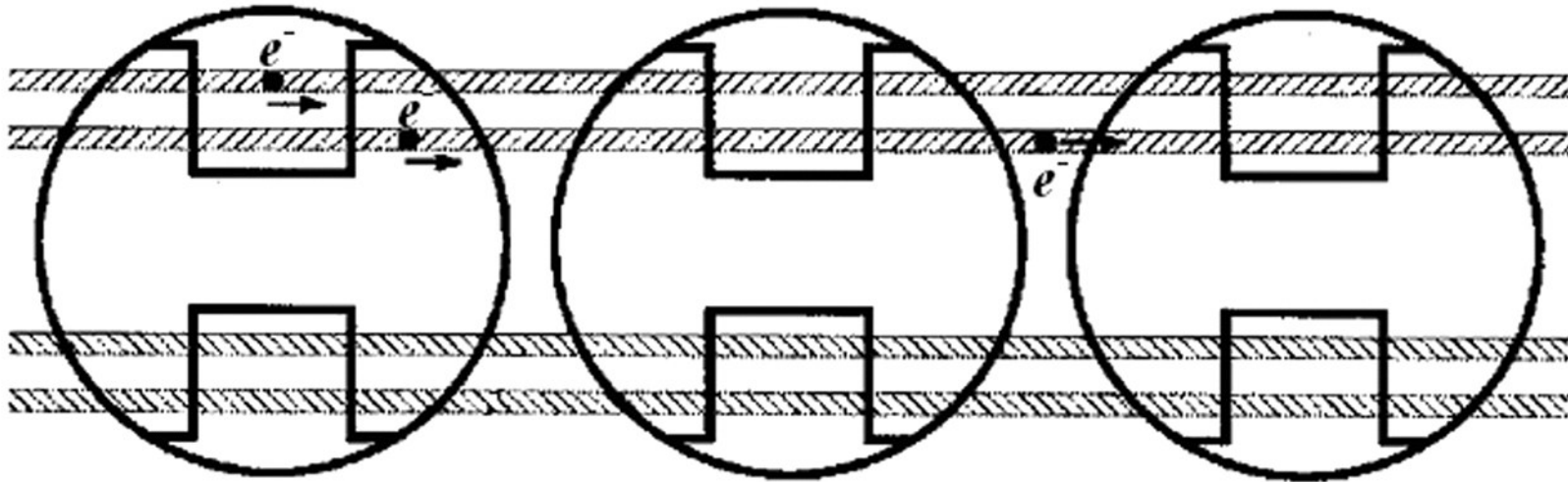
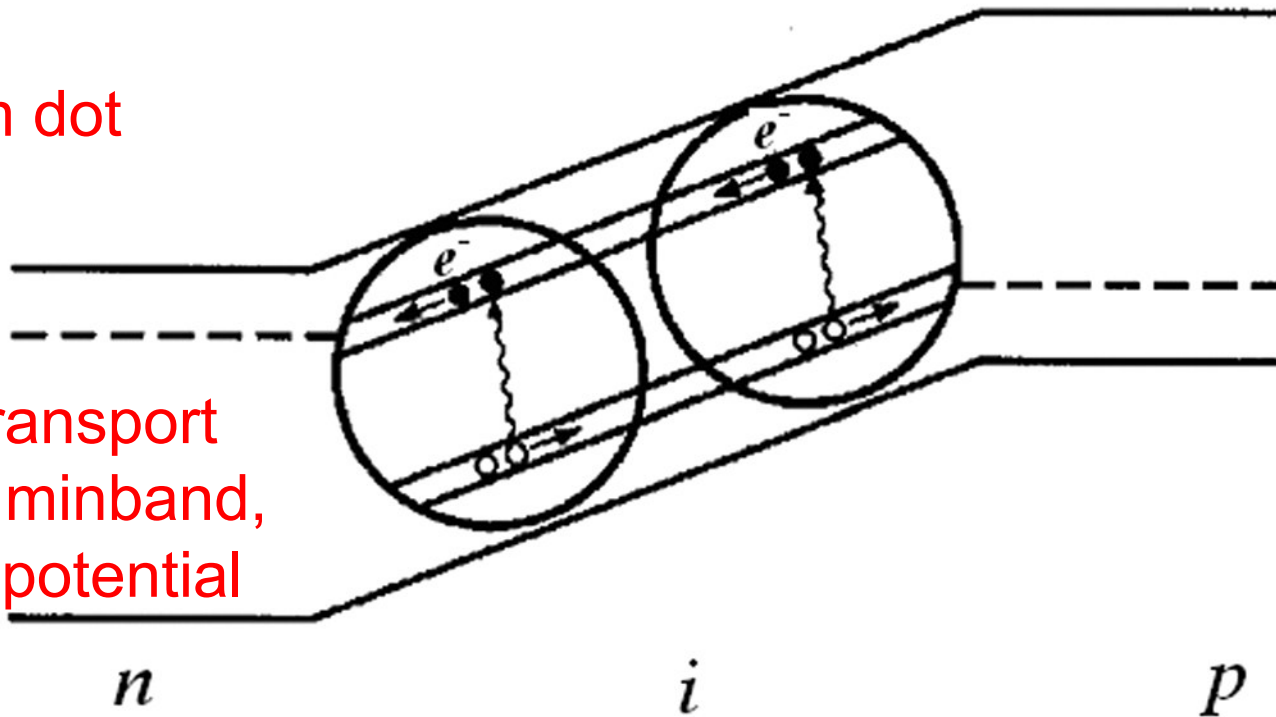


Figure 10.25
 © John Wiley & Sons, Inc. All rights reserved.

(a) bilayer, (b) bulk heterojunction



Quantum dot
solar cell



Carrier transport
through miniband,
a higher potential

Figure 10.26a

Reprinted from *Physica E: Low-Dimensional Systems and Nanostructures*, 14, A.J. Nozik, "Quantum dot solar cells", pp. 115-120, Copyright 2002, with permission from Elsevier.

Impact ionization enhances efficiency

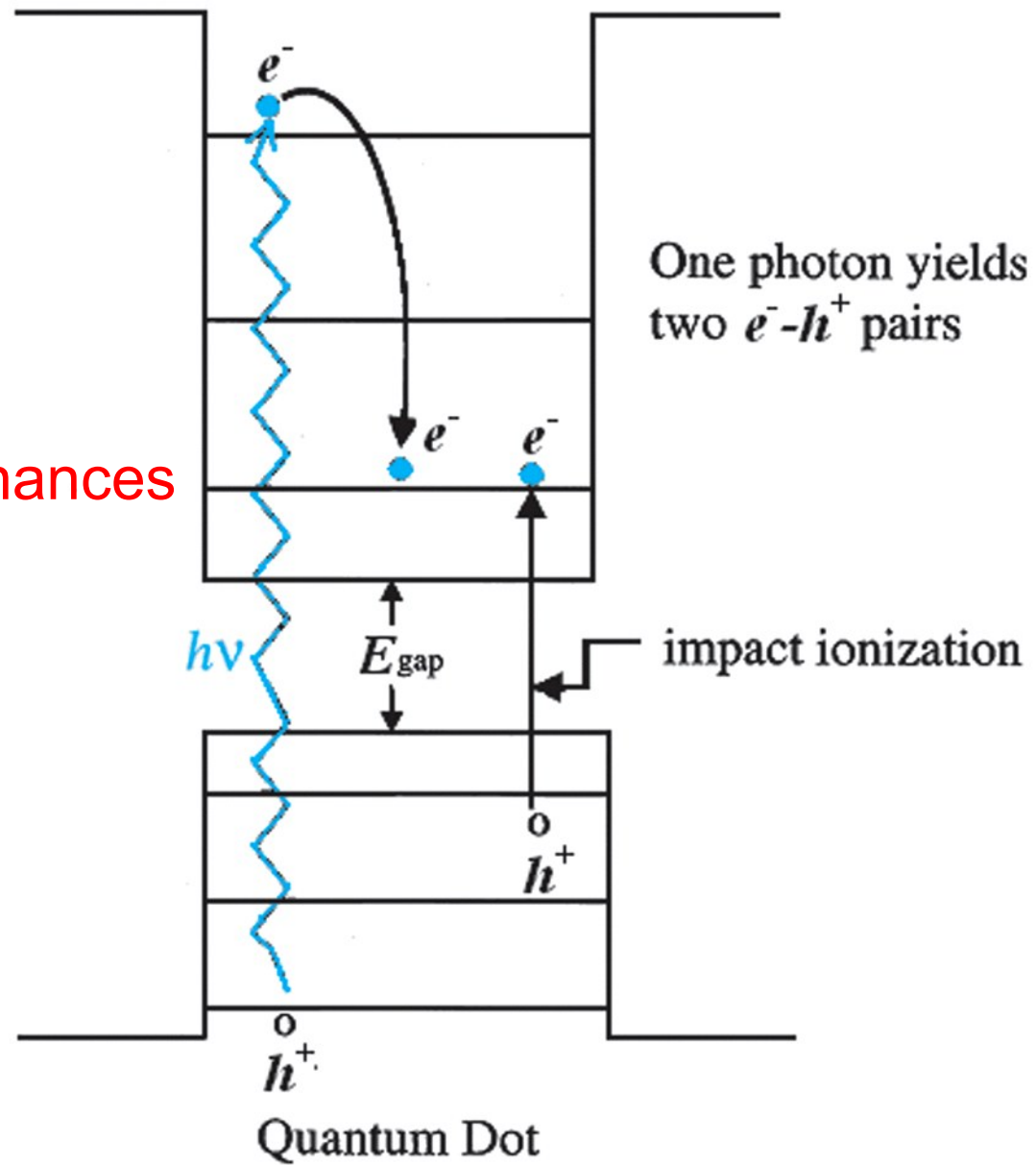


Figure 10.26b

Reprinted from *Physica E: Low-Dimensional Systems and Nanostructures*, 14, A.J. Nozik, "Quantum dot solar cells", pp. 115-120, Copyright 2002, with permission from Elsevier.

Efficiency, open-circuit voltage, short-circuit current, and fill factor versus solar concentration.³⁰

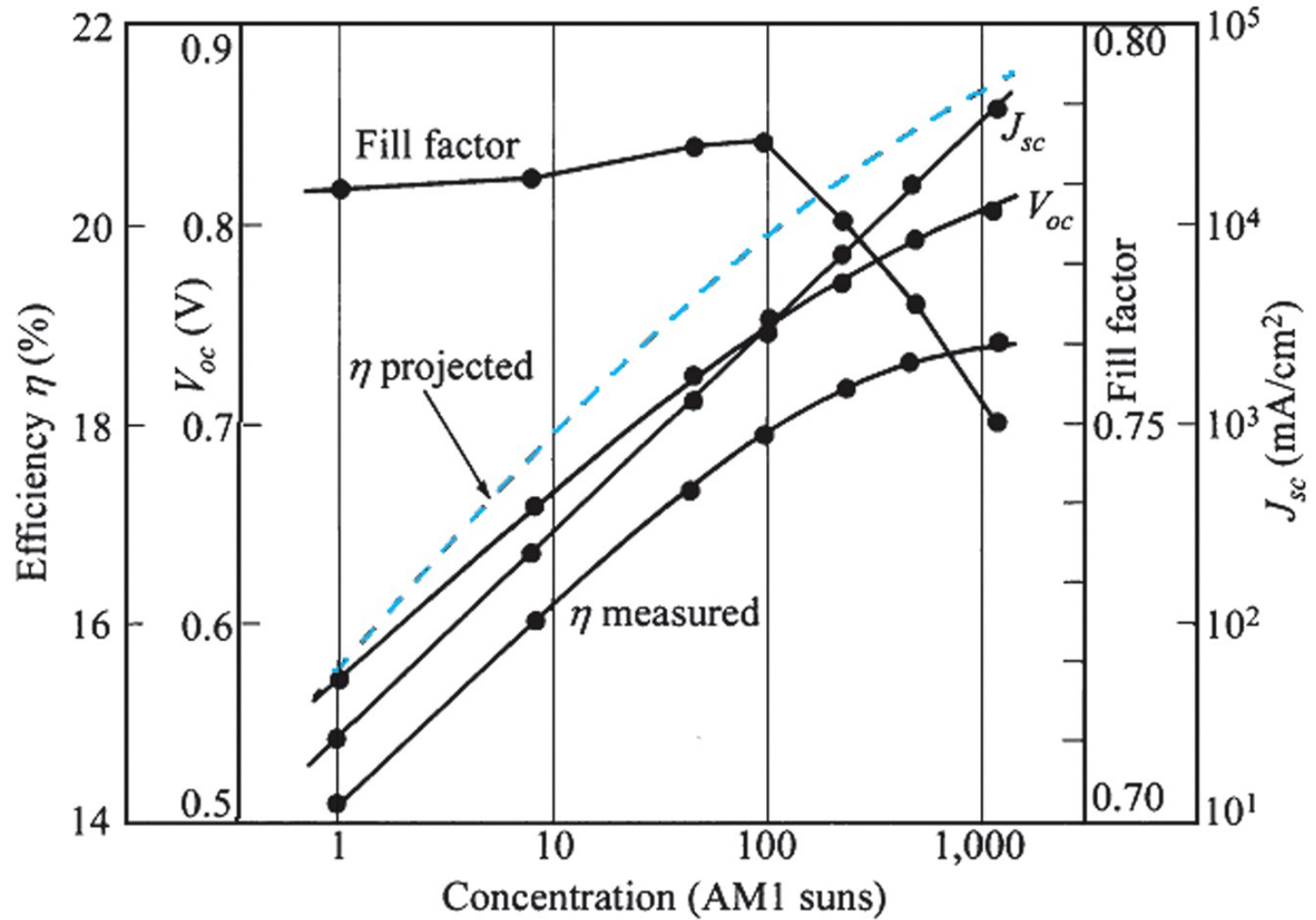


Figure 10.27
© John Wiley & Sons, Inc. All rights reserved.

聚光increase η , V_{oc} 等優點 強度上升1E3